

MIT Open Access Articles

Environmental conditions and microbial community structure during the Great Ordovician Biodiversification Event; a multi-disciplinary study from the Canning Basin, Western Australia

The MIT Faculty has made this article openly available. **Please share** how this access benefits you. Your story matters.

Citation: Spaak, Gemma et al. "Environmental conditions and microbial community structure during the Great Ordovician Biodiversification Event; a multi-disciplinary study from the Canning Basin, Western Australia." *Global and Planetary Change* 159 (December 2017): 93-112 © 2017 Elsevier B.V.

As Published: <http://dx.doi.org/10.1016/j.gloplacha.2017.10.010>

Publisher: Elsevier BV

Persistent URL: <https://hdl.handle.net/1721.1/128454>

Version: Author's final manuscript: final author's manuscript post peer review, without publisher's formatting or copy editing

Terms of use: Creative Commons Attribution-NonCommercial-NoDerivs License



Environmental conditions and microbial community structure during
the Great Ordovician Biodiversification Event; a multi-disciplinary
study from the Canning Basin, Western Australia

Gemma Spaak^a, Dianne S. Edwards^b, Clinton B. Foster^c, Anais Pagès^{d,a}, Roger E. Summons^e,
Neil Sherwood^f, Kliti Grice^{a*}

^a*Western Australian Organic and Isotope Geochemistry Centre (part of The Institute for
Geoscience Research), Curtin University, Perth, WA 6845, Australia*

^b*Geoscience Australia, Canberra, ACT 2609, Australia*

^c*School of Earth and Environment, The University of Western Australia, Perth, WA 6009,
Australia*

^d*CSIRO Mineral Resources, Perth, WA 6151, Australia*

^e*Department of Earth, Atmospheric & Planetary Sciences, MIT, Boston, USA*

^f*CSIRO Energy, Sydney, NSW 2113, Australia*

*Corresponding author:

Kliti Grice

Curtin University

WA-OIGC – Dept. of Chemistry

GPO Box U1987

Perth, WA 6102 Australia

Phone: +61 (0)8 9266 2474

Email address:

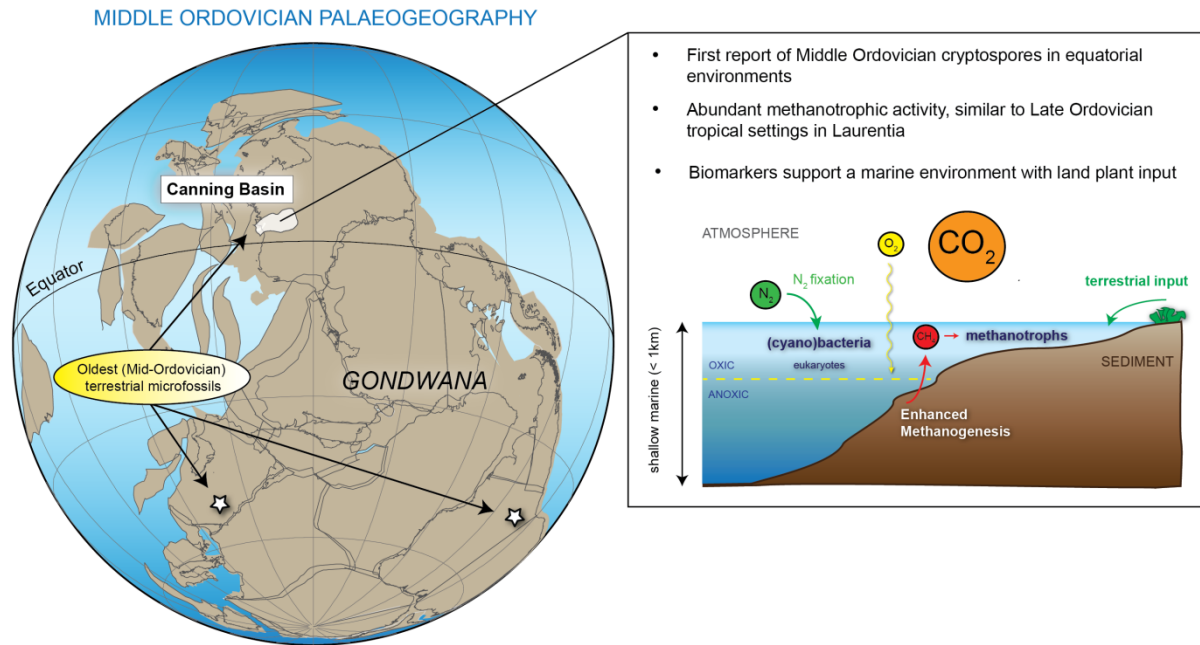
K.Grice@curtin.edu.au

Abstract

The Great Ordovician Biodiversification Event (GOBE) is regarded as one of the most significant evolutionary events in the history of Phanerozoic life. The present study integrates palynological, petrographic, molecular and stable isotopic ($\delta^{13}\text{C}$ of biomarkers) analyses of cores from four boreholes that intersected the Goldwyer Formation, Canning Basin, Western Australia, to determine depositional environments and microbial diversity within a Middle Ordovician epicontinental, tropical sea. Data from this study indicate lateral and temporal variations in lipid biomarker assemblages extracted from Goldwyer Formation rock samples. These variations likely reflect changing redox conditions between the upper (Unit 4) and lower (Units 1+2) Goldwyer, which is largely consistent with existing depositional models for the Goldwyer Formation. Cryptospores were identified in Unit 4 in the Theia-1 well and are most likely derived from bryophyte-like plants, making this is the oldest record of land plants in Australian Middle Ordovician strata. Biomarkers in several samples from Unit 4 that also support derivation from terrestrial organic matter include benzonaphthofurans and $\delta^{13}\text{C}$ -depleted mid-chain *n*-alkanes. Typical Ordovician marine organisms including acritarchs, chitinozoans, conodonts and graptolites were present in the lower and upper Goldwyer Formation, whereas the enigmatic organism *Gloeocapsomorpha prisca* (*G. prisca*) was only detected in Unit 4. The correlation of *G. prisca* with high 3-methylhopane indices and ^{13}C -depleted *G. prisca* biomarkers is interpreted to suggest an ecological relationship between methanotrophs and *G. prisca*. This research contributes to a greater understanding of Ordovician marine environments from a molecular perspective since few biomarker studies have been undertaken on age-equivalent sections. Furthermore, the identification of the oldest cryptospores in Australia and their corresponding terrestrial biomarkers provides further insight into the geographical evolution of early land plants.

Keywords: Darriwilian, Canning Basin, biomarkers, methanotrophs, *Gloeocapsomorpha prisca*, cryptospores

Graphical Abstract



1 Introduction

The Ordovician Period is a unique time in Earth's history, with characteristically high sea levels and a major increase in marine biodiversity (e.g. Cooper and Sadler, 2004). This rise in biodiversity is commonly referred to as the Great Ordovician Biodiversification Event (GOBE) which, together with the Cambrian Explosion, were the most significant Paleozoic evolutionary events (Cooper and Sadler, 2004; Harper, 2006; Servais et al., 2009). The GOBE has been extensively studied using the fossil record, but far less is known about the biomarker assemblages of Middle Ordovician marine depositional environments. The Darriwilian Goldwyer Formation (Fig. 1, Fig. 2) of the Canning Basin, Western Australia, is one of a few examples of Middle Ordovician sediments on the Australian continent deposited in an equatorial inland sea containing a prolific and diverse microfossil assemblage (Quintavalle and Playford, 2008, 2006; Winchester-Seeto et al., 2000).

During the Ordovician, sea levels were probably higher than at any other time in the Paleozoic (Munnecke et al., 2010) and the expansion of marine habitats was an important stimulus for the diversification. Although the rise in biodiversity predominantly applied to marine organisms, life on land also started to evolve during this time. The Middle Ordovician (Dapingian) records the earliest evidence of land plants in the form of cryptospores—microfossils of presumed bryophyte origin (Rubinstein et al., 2010). These early plants resemble bryophytes in their size and morphology, but their biology remains largely unknown (Edwards et al., 2014). Recent work by Lenton et al. (2016, 2012) suggests that the appearance of early land plants could have had a significant impact on global climate, potentially contributing to the Late Ordovician cooling and the rise in atmospheric oxygen.

Biomarkers are useful reconstruction tools which provide detailed information on past microbial communities, terrestrial inputs in marine environments, as well as other palaeoenvironmental conditions such as water column chemistry and stratification (e.g. Peters et al., 2005). Most Ordovician marine species are now extinct and the study of biomarkers,

molecular compounds with specific biosynthetic origins, can reveal further information on the physiology and ecology of these extinct species (e.g. Hoffman et al., 1987; Blokker et al., 2001; Gupta et al., 2006; Dutta et al., 2007; Jacob et al., 2007). Of particular interest is *Gloeocapsomorpha prisca* (*G. prisca*), an organic-walled microfossil of controversial habitat and physiology, which exhibits characteristic geochemical properties and has contributed to many Cambro-Ordovician organic-rich rocks (e.g. Reed et al., 1986; Foster et al., 1986, 1989, 1990; Fowler et al., 2004). Biomarkers also have the potential to identify organisms that are rarely preserved as fossils, such as 3-methylhopanes which are pertinent to detect the presence of methanotrophs (e.g. Farrimond et al., 2004 and references therein). Coupling biomarker studies with compound-specific isotope analyses can provide further insight into organic matter sources, microbial communities and biogeochemical cycles.

The primary aim of the present study is to provide further understanding of Middle Ordovician microbial community structure from a molecular perspective. The Goldwyer Formation is an analogue for Middle Ordovician epeiric tropical environments, and the multi-disciplinary approach allows for integration of molecular signatures with micro- and macrofossils. This paper presents data from molecular and compound-specific stable isotopic ($\delta^{13}\text{C}$ of biomarkers) analyses together with palynological and petrological studies to understand the relationships between palaeoenvironment, microbial communities and the type of organic matter preserved within the marine sediments.

2 Geological background

The Canning Basin, located in the northwestern part of Western Australia (WA) (Fig. 1), is the largest onshore sedimentary basin in this state covering an area of about 430,000 km² (Triche and Bahar, 2013). The basin contains rocks of Ordovician to Cretaceous age (Forman and Wales, 1981; Kennard et al., 1994). Deposition in the Canning Basin began in the Early Ordovician as a consequence of extensional tectonics, with rapid subsidence during the Early–Middle Ordovician resulting in the onset of marine conditions (Romine et al., 1994). Macro- and microfossils from the Middle Ordovician Goldwyer Formation corroborate a shallow marine depositional environment (Haines, 2004; Quintavalle and Playford, 2008, 2006; Winchester-Seeto et al., 2000). By the Late Ordovician, subsidence ceased and marginal marine and evaporitic conditions were established. Smaller scale transgressive-regressive cycles are superimposed on this broad regional trend (Haines, 2004).

Four informal lithologic units (designated Units 1 to 4) have been described for the Goldwyer Formation by Foster et al. (1986) in the eastern Canning Basin. Palynological assemblage zones roughly correlate to these lithological units (Quintavalle and Playford, 2006), as shown in Figure 2. In a sequence stratigraphic framework, the lower Goldwyer succession (Units 1+2) records a major transgression affecting most of the basin that deposited open marine mudstones over 700 m thick in basinal areas and condensed-section carbonates on platforms and terraces. The onset of the transgression is shown by an abrupt increase in petrophysical borehole electric-log measurement of gamma radiation in Goldwyer-1 and Theia-1 (Fig. 1). The transgression was followed by a slow regressive phase with the deposition of outer shelf to fore slope facies (Romine et al., 1994; Haines, 2004). A smaller scale regression resulted in the deposition of a carbonate-dominated succession (Unit 3), followed by another transgression with the deposition of the upper Goldwyer Formation (Unit 4), that can also be observed in the gamma-ray logs (Fig. 1).

For the present study, the lower and upper calcareous mudstone units of the Goldwyer Formation were sampled in four wells from west to east: Goldwyer-1, Theia-1, Santalum-1A and Solanum-1. Solanum-1 and Santalum-1A intersect a more limestone-dominated succession in comparison to the mudstone-dominated sediments intersected in Goldwyer-1, and Theia-1, especially in relation to Unit 4, indicating shallower conditions on the more southwestward part of the Broome Platform (Haines, 2004). The carbonates from Unit 4 in Solanum-1 and Santalum-1A are bioturbated whereas the samples from Units 1+2 and Unit 4 in Goldwyer-1 and Theia-1 comprise grey-black mudstone with no obvious bioturbation. Further sample description is provided in the supplementary online material (SOM).

3 Materials and Methods

3.1 Sampling strategy and preparation

To investigate the depositional environment of the Goldwyer Formation, cores from Goldwyer-1, Santalum-1A, Solanum-1 and the recently drilled well, Theia-1 (Finder Exploration Pty Ltd, 2015) were sampled. Sample selection was based on: availability of core; previously measured total organic carbon (TOC) contents (> 1 wt. %); and, for three wells, evidence of low thermal maturity from previously measured Rock-Eval data and maceral reflectance values. Organic matter from Theia-1 is the most thermally mature, and samples with high TOC were selected. As noted above, four informal rock units have been recognised in the Goldwyer Formation (Units 1 to 4). Unit 3, composed predominantly of carbonate, was not sampled due to its low TOC contents. Unit 4 (upper Goldwyer Formation) was sampled more frequently based on previous records of the distinctive palynomorph *G. prisca*. Sample material was obtained from core stored at the Geological Survey of Western Australia core library. Ensuring hydrocarbon syngeneity in ancient rocks is crucial

to avoid misinterpretation of the biomarker signatures (e.g. Brocks et al., 2003). Once the cut core samples were obtained from the core library they were wrapped in aluminium foil to minimise further surface contamination. Rock samples were surface washed several times with organic solvents to remove surface contamination prior to grinding. Procedural blanks were adopted throughout the washing, grinding and extraction process to avoid (cross) contamination. The protocol for sample preparation and extraction is described in detail in the SOM.

3.2 Analytical methods

Rock-Eval pyrolysis, organic petrology, palynology and organic geochemical analyses were undertaken following published, standardised methods which are described in the SOM.

4 Results and Interpretation

4.1 Palynology

Palynological analyses were carried out on selected samples from Units 1+2 and Unit 4 in all four wells. Palynomorph assemblages and key species are summarised in Table 1 and shown in Figure 3. The results indicate a marine depositional environment with evidence of land-plant input in Unit 4.

The marine microfossils include: graptolite fragments (Goldwyer-1), chitinozoans, scolecodonts (worm jaw fragments commonly associated with bioturbated sediments), spinose acritarchs, and *G. prisca* colonies (Theia-1, Santalum-1A and Solanum-1) (Fig. 3). All acritarch species have been reported previously by Quintavalle and Playford (2006). Winchester-Seeto et al. (2000) provide a more detailed account concerning the association

and quantitative abundances of these fossil groups which reflect small scale transgressive-regressive cycles in Unit 4 of Santalum 1A.

Cryptospores were found in Unit 4 of Theia-1 (1217.67–1217.7 m), being preserved as dyads and tetrads, both naked and enclosed in an envelope. These tetrads exhibit strong similarities to an undescribed Dapingian cryptospore previously identified in samples from Argentina (Rubinstein et al., 2010). One spore specimen appears to exhibit a trilete mark (Fig. 3h), but within this specimen the trilete mark is thicker than those reported by Steemans et al. (2009) and does not clearly extend towards the outer rim. However, if this is a true trilete spore, it would predate the current oldest occurrence of trilete spores (late Katian/Hirnantian) by ca. 20 Ma (Steemans et al., 2009).

4.2 Organic Petrology

Organic petrological analyses undertaken in both white light and ultraviolet light showed that the macerals in Unit 4 at Solanum-1 and Santalum-1A comprise common fluorescing liptinite and rare vitrinite-like faunal remains, probably derived from graptolites (Sherwood and Li, 2016), as shown in Figure 4. The liptinite in most samples from Solanum-1 comprised acritarch-derived lamalginite, along with lesser amounts of liptodetrinite and telalginite derived from *G. prisca* (Fig. 4b-c; Table 2). Liptinite in the lowermost sample (~490 m depth) from Santalum-1A occurs mainly as telalginite, derived from *G. prisca* (Fig. 4a), along with sparse acritarch-derived lamalginite.

The uppermost sample (973 m) from Unit 4 in Goldwyer-1 contained rare fluorescing liptodetrinite and lamalginite derived from acritarchs. In contrast, the organic matter in the samples from Units 1+2 comprised non-fluorescing, finely disseminated bitumen with rare to sparse vitrinite-like faunal remains exhibiting characteristics similar to that of chitinozoans and graptolites (Fig. 4d).

4.3 Organic richness and thermal maturity

Rock-Eval pyrolysis results are summarised in Table 2. The Goldwyer Formation samples from Unit 4 contained type II kerogen with TOC content up to 3.6 wt. %. Maceral reflectances ranged between 0.5 and 0.7%, indicating thermal maturities within the early stage of oil generation. The organic matter preserved in Units 1+2 at Goldwyer-1 and Theia-1 also classified as type II kerogen with maximum TOC contents of 4.5 wt. % (Fig 1). Slightly higher thermal maturities are observed in these samples (maceral reflectance of 0.8–1.5%). In Theia-1, maceral reflectance values are >1% and the absence of hopanes and steranes corroborate high thermal maturity (in the main stage of gas generation).

4.4 Aliphatic and aromatic hydrocarbons

All aliphatic hydrocarbon fractions contained abundant short to mid chain length *n*-alkanes (C₁₂ [occasionally], C₁₄ to C₂₃), with some samples showing additional contributions of longer *n*-alkanes (up to C₃₃) (Fig. 5). The isoprenoids pristane (Pr) and phytane (Ph) were consistently present but varied in abundance throughout the samples (Fig. 5). The C₂₇–C₃₅ hopanes and C₂₆–C₃₀ steranes were below detection limit in full scan GC-MS analysis and were identified using selected ion monitoring (SIM) mode and multiple reaction monitoring (MRM) GC-MS (Fig. 6, S1, S2, S3 and S4). The aromatic hydrocarbon fractions were dominated by naphthalene, phenanthrene and their methylated derivatives. A detailed account of the *n*-alkane, hopane and sterane assemblages and aromatic compounds is provided in the SOM. Compound specific carbon isotope ($\delta^{13}\text{C}$) analysis was performed upon *n*-alkanes from selected samples (Table 5). Samples from Units 1+2 displayed slightly lower *n*-alkane $\delta^{13}\text{C}$ values (-31.3 to -33.8‰) than samples from Unit 4 (-27.1 to -32.3‰). In Unit 4 of Santalum-

232 1A, the C₁₄-C₂₀ *n*-alkanes were more enriched (-27.1 to -29.4‰) than the C₂₅-C₃₂ *n*-alkanes (-
233 29.9 to -32.3‰). Trends in the $\delta^{13}\text{C}$ values are illustrated in Figure 10, 12 and S5. The most
234 important molecular and isotopic signatures are summarised in Table 3, together with their
235 biological and environmental interpretation.

236

5 Discussion

5.1 Evidence of water-column stratification and anoxia

Molecular proxies indicative of environmental conditions are displayed in Fig. 7 and listed in Table 4. The Pr/Ph ratio, dibenzothiophene/phenanthrene (DBT/P) ratio and C₃₅ homohopane index are commonly used redox indicators (Didyk et al., 1978; Hughes et al., 1995; Peters et al., 2005). An elevated gammacerane index is indicative of a stratified water column (Moldowan et al., 1985; Sinninghe Damsté et al., 1995; Tulipani et al., 2015b). The samples from Unit 4 in Santalum-1A and Solanum-1 on the eastern part of the Broome Platform, contained low gammacerane indices (<0.1) and low C₃₅ homohopane indices (average of 0.04) (Fig. 7), suggesting deposition under relatively oxygenated conditions with enhanced water column circulation, which is corroborated by the presence of bioturbation in these sediments.

Although there are fewer data from Units 1+2 in comparison to Unit 4, these samples displayed higher gammacerane indices (0.3–0.7) (Fig. 7) and slightly higher C₃₅ homohopane indices (average of 0.06). However, the Pr/Ph ratio and DBT/P ratio do not exhibit distinct differences between Unit 4 and Units 1+2 (Fig. 7). Nonetheless, due to sedimentological features such as laminations and only occasional bioturbation, deposition of Units 1+2 likely occurred under less oxygenated conditions. Deposition of Units 1+2 occurred during a maximum transgression (Romine et al., 1994) and sedimentological features such as high TOC content, laminations and only occasional bioturbation suggests anoxic bottom waters. In this case, decreased oxygenation is likely a result of deeper water conditions facilitated by the transgression. However, this hypothesis does not account for topographic variations along the Broome Platform. Silty lenses in the upper part of Units 1+2 at Theia-1 suggest wave action on a muddy shelf. Due to the size of the basin, distance between sampled wells and the low

sampling density of Units 1+2, it remains difficult to infer relationships between molecular redox proxies and the geological framework.

The presence of hydrogen sulfide within the sunlight zone of the water column and/or at the sediment/water interface is known as photic zone euxinia (PZE). Phototrophic sulfur bacteria such as Chlorobiaceae flourish in such conditions (Grice et al., 2005; Schwark and Frimmel, 2004). Commonly used biomarkers of Chlorobiaceae include chlorobactane, isorenieratane, palaerenieratane and their derivatives the aryl isoprenoids with corresponding enriched $\delta^{13}\text{C}$ values (Summons and Powell, 1987; Grice et al., 1996). Biomarkers for PZE have been identified in some (restricted) Ordovician-Silurian settings (Koopmans et al., 1996; Pancost et al., 1998; Vandenbroucke et al., 2009; Smolarek et al., 2017). In this study, trace amounts of palaerenieratane and isorenieratane were identified in Solanum-1 at 316.2–316.3 m and in Theia-1 at 1552.7–1552.75 m and aryl isoprenoids of uncertain origin in others (SOM). The low abundance of aryl isoprenoids and aromatic C_{40} carotenoids possibly suggest short periods of PZE, but mixing and oxygenation of the water column must have been frequent to prevent the development of PZE for prolonged periods of time.

5.2 Microbial communities inferred from hopane and sterane distributions

The ratio of the C_{27} to C_{35} hopanes to C_{27} to C_{29} steranes (H/St) generally reflects the balance of bacterial *versus* eukaryotic contributions to sedimentary organic matter. Hopanes are the molecular fossils of hopanoids produced by diverse groups of bacteria, whilst steranes are derived from sterols common to all eukaryotes and are generally absent in bacteria, with few exceptions (Summons et al., 2006; Volkman, 2006, 1986). Further information on bacterial and algal populations can be obtained from the distributions and relative abundances of the C_{31} 2 α - and 3 β -methylhopanes and the C_{27} , C_{28} and C_{29} steranes. Figure 7 shows variations in the H/St ratios *versus* methylhopane abundance between Units 1+2 and Unit 4.

289 In Unit 4, high H/St ratios (H/St average of 6.7) were observed, reflecting a strong
290 predominance of bacteria. These values are significantly above the global average (0.5–2.0)
291 of Phanerozoic marine oils and sediments (Peters et al., 2005). During the Ordovician, fixed
292 nitrogen content of the oceans was low due to extensive denitrification (LaPorte et al., 2009;
293 Melchin et al., 2013; Rohrssen et al., 2013). Eukaryotic algae commonly require a steady
294 supply of fixed nitrogen, and such environmental conditions would have limited their
295 presence in Ordovician oceans (LaPorte et al., 2009). Unit 4 also exhibited high 3-
296 methylhopane abundances, illustrated by high 3-methylhopane indices and low 2-
297 methylhopane/3-methylhopane ratios (Fig. 7, Table 4). Both methanotrophic bacteria and
298 acetic acid bacteria have the ability to produce 3-methylhopanoids (Farrimond et al., 2004;
299 Welander and Summons, 2012), but the presence of acetic acid bacteria would be unlikely in
300 such carbonate-rich, marine environments. The high 3-methylhopane abundance in Unit 4 is
301 interpreted to be indicative of aerobic methanotrophic bacteria, which is consistent with the
302 relatively oxygenated character of the water column under which the sediments within
303 Santalum-1A and Solanum-1 were deposited. Methanotrophic bacterial activity implies the
304 presence of methane in aerobic waters. An enhanced methane cycle has been proposed by
305 Rohrssen et al., (2013) and is thought to have facilitated the presence of methanotrophs. In
306 marine sediments characterised by low concentrations of oxygen and other electron acceptors
307 such as nitrate and sulfate, methanogenesis can account for a significant proportion of organic
308 matter diagenesis. Under such conditions anaerobic oxidation of methane via either sulfate or
309 nitrate reduction would have been low, allowing a greater proportion of methane to escape
310 from the sediments into the water column. In comparison to the present-day, Ordovician
311 oceans were characterised by low concentrations of oxygen, nitrate and sulfate (Gill et al.,
312 2007; Hammarlund et al., 2012; LaPorte et al., 2009; Thompson and Kah, 2012) and
313 diagenetic methane cycling likely played an important role during deposition of the upper
314 Goldwyer Formation, signified by the abundance of methanotrophic bacteria, especially in

Unit 4. A graphical representation of the microbial community present during deposition of Unit 4 is provided in Figure 9.

The samples from Units 1+2 displayed significantly lower H/St ratios (<2) compared to Unit 4, accompanied with relatively elevated 2-methylhopane abundances. Enhanced levels of fixed nitrogen could have resulted from greater cyanobacterial contributions shown by the relatively elevated 2-methylhopane abundance (Farrimond et al., 2004; Summons et al., 1999; Summons and Jahnke, 1990). This could have enhanced algal productivity, reflected in the lower H/St ratios. Although the presence of 2-methylhopanes in sediments is often correlated to cyanobacteria, several other modern-day bacteria are known to produce 2-methylhopanoids (Ricci et al., 2014) which inhabit a multitude of modern environments. These environments are characterised by suboxia or anoxia, high osmolarity and limited fixed nitrogen (Ricci et al., 2014), which is in agreement with the reducing character of Units 1+2. In this case, the high relative 2-methylhopane abundance can reflect both an increase in cyanobacterial abundance and low oxygen levels.

Steranes are biomarkers for algae and most likely acritarchs (e.g. Talyzina et al., 2000; Volkman, 2006). Acritarch microfossils have been identified in Unit 4 (Table 1) in this study and in previous studies of the Goldwyer Formation (Quintavalle and Playford, 2006; Winchester-Seeto et al., 2000). The absence of acritarch microfossils in samples from Units 1+2 in this study may be due to sampling bias because relatively few samples were subjected to palynological analysis. Thus, the sterane assemblages are inferred to be indicative of algal as well as acritarch contributions to the biomass in Units 1+2 and Unit 4. Common steranes (C_{27} , C_{28} and C_{29}), dinosteranes and 4α -methyl-24-ethylcholestanes have been identified in numerous acritarch microfossils (e.g. Arouri et al., 2000; Talyzina et al., 2000). Dinosterane ($4\alpha,23,24$ -trimethylcholestane) and 4α -methyl-24-ethylcholestanes were detected in selected samples from Units 1+2 and Unit 4 at varying abundances (Fig. 6), which could potentially be related to different acritarch communities.

The C₂₇:C₂₈:C₂₉ sterane distribution in Early Palaeozoic marine deposits is generally characterised by equal amounts of C₂₇ and C₂₉ steranes or a predominance of C₂₉ steranes (Grantham and Wakefield, 1988; Schwark and Emt, 2006;), although, a strong predominance of C₂₇ steranes has been noted in certain Late Ordovician marine sections (Mustafa et al., 2015; Smolarek et al., 2017). In the upper Goldwyer, the percentages of C₂₇ steranes (of C₂₇₋₂₉ steranes) vary from ca. 30% to 50%, the percentages of C₂₈ steranes vary from ca. 14% to 27%, and the percentages of C₂₉ steranes vary from ca. 22% to 52%. Lateral variations are evident in the C₂₇:C₂₈:C₂₉ sterane distribution throughout Unit 4 (Fig. 8), but these do not correlate with other biomarker proxies. In the lower Goldwyer Formation the percentage of C₂₉ steranes is slightly higher (ca. 46% to 54%) providing further indication that different microbial communities were present during deposition of Units 1+2 and Unit 4.

5.3 *Gloeocapsomorpha prisca*

Microfossils characteristic of *G. prisca* were identified in Unit 4 of Theia-1, Solanum-1 and Santalum-1A (Fig. 2, Fig. 3, Table 1). Hydrocarbon fractions of *G. prisca*-rich rocks typically contain distinctive odd-carbon-numbered *n*-alkanes in the C₁₅ to C₁₉ range with minor contributions of C₂₀₊ *n*-alkanes, abundant odd-carbon-numbered *n*-alkylcyclohexanes, very low contributions of acyclic isoprenoid hydrocarbons, a strong predominance of hopanes *versus* steranes and abundant long-chain alkyl naphthalenes and alkylbenzenes (e.g. Fowler et al., 2004; Guthrie and Pratt, 1995; Hoffmann et al., 1987). The typical odd-over-even *n*-alkane signature of *G. prisca* was observed in selected Unit 4 samples from Theia-1, Santalum-1A and Solanum-1, with varying abundance. For example, the *n*-alkane OEP was clearly present at the base of Unit 4 for Solanum-1 (Fig. 5a), less abundant in the Theia-1 samples (likely due to higher maturity) (Fig. 5e) and absent in the Santalum-1A samples. Because *n*-alkanes are found in virtually all extant organisms (Brocks and Summons, 2014)

and no major maturity variations exist between Solanum-1 and Santalum-1A, contributions of other organic matter sources most likely account for the absence of an OEP in the Santalum-1A samples. Comparison of *n*-alkane profiles from Solanum-1 samples where *G. prisca* has been quantified microscopically (based on visual estimates) showed that the *n*-alkane OEP only became prominent when the *G. prisca* liptinite visual abundance was at least 5% of the sample. The $\delta^{13}\text{C}$ values of *n*-alkanes in the Solanum-1 samples showed a shift towards more depleted carbon isotopic signatures (Fig. 8 and Fig. 10). In addition, the *n*-alkane isotopic profile of these samples show that the odd-carbon numbered *n*-C₁₇ and *n*-C₁₉ were more depleted in ¹³C (-31.4‰) in comparison to *n*-C₁₆ and *n*-C₁₈ (-30.0‰) (Fig. 11). These results suggest that the depleted isotopic signature is related to the aliphatic biopolymer of *G. prisca*, which is the predominant source of *n*-C₁₇ and *n*-C₁₉.

In Unit 4 of Solanum-1, high abundances of *G. prisca*, shown as a pronounced OEP, correlated with TOC abundance equal or greater than 1 wt. %, Pr/Ph ratios >1, lower C₃₅ homohopane indices, elevated H/St ratios, increased 3-methylhopane indices and depleted carbon isotopic signatures of the individual *n*-alkanes (Fig. 8). Furthermore, intervals were characterised by a change in sedimentation from carbonate to mud-dominated and bioturbation became less prominent, as observed in the hylogged core section (Fig. S6). Elevated TOC contents indicate anoxic bottom waters. The disparity between elevated TOC contents and relatively high Pr/Ph ratios and low homohopane indices has been noted previously in the *G. prisca*-rich Guttenberg Member from Iowa (Pancost et al., 1998). In the Guttenberg Member, *G. prisca* makes up 45 to 95 % of the organic matter and it is argued that dense layers of *G. prisca* limited the production of sedimentary hydrogen sulfide. This would have enhanced the preservation of phytol and bacteriohopanetetrol, rationalising relatively high Pr/Ph ratios and low homohopane indices in comparison to sections above and below the Guttenberg Member (Pancost et al., 1998). In this study, *G. prisca* abundances are much lower and such an explanation cannot be employed. Marine carbonates are commonly

associated with high homohopane indices (Peters et al., 2005) and a change from carbonate- to mud-dominated sedimentation is likely driving the observed shift in homohopane index. Likewise, variations in source inputs to Pr and Ph are thought to account for the slight increase in Pr/Ph ratio. Anoxic to dysoxic bottom waters would have promoted methanogenesis and subsequently increased the methane flux into the water column, allowing for an increase in methanotrophs, reflected in increased 3-methylhopane indices (Fig. 8). Rapid sedimentation and burial of refractory *G. prisca* microfossils likely resulted in preservation of organic matter in a predominantly oxygenated water column.

Lipids derived from aerobic methanotrophs are known to be significantly depleted in $\delta^{13}\text{C}$ (Summons et al., 1994). In Unit 4 of Solanum-1, the co-occurrence of (i) *G. prisca* biosignatures, (ii) increased 3-methylhopane indices and (iii) depleted carbon isotopic signatures (Fig. 8) suggests a relationship between *G. prisca* and methanotrophs. In Iowa *G. prisca* biomass is significantly enriched in ^{13}C relative to that of other photoautotrophic organisms (Pancost et al., 1999) and *G. prisca*-rich bitumens from North America exhibit enriched $\delta^{13}\text{C}$ values for *n*-C₁₇ and *n*-C₁₉ relative to the even numbered *n*-alkanes, which is opposite to the Solanum-1 samples (Fig. 11). In Iowa equal amounts of 3- and 2-methylhopanes were recorded (Pancost et al., 1998), whereas the Solanum-1 rock extracts show a distinct predominance of 3-methylhopanes (3MHI of 9-15%) relative to the 2-methylhopanes (2MHI of 3-7%) (Fig. 8). Hence, it seems likely that *G. prisca* utilised carbon ultimately derived from either methane or aerobic methanotrophs resulting in ^{13}C -depleted *n*-alkanes. Similar *n*-alkane carbon isotopic profiles (as shown in Fig. 11) are noted in oils sourced by *G. prisca* in the Canning and Amadeus Basins (Edwards et al., 2013; Jarrett et al., 2016) and a predominance of 3- versus 2-methylhopane is recorded in one of the oils from the Canning Basin (Edwards et al., 1995). These results suggest that the association between methanotrophs and *G. prisca* may not have been a local phenomenon. Although the uptake of ^{13}C depleted carbon via methanotrophs is thought to be the most plausible explanation for the

observed isotopic shifts in Solanum-1, other processes (e.g. recycling of CO₂) may have played a role. Nonetheless the carbon isotopic variations in Australia and North America (Fig. 11) are significant and further investigation is needed to elucidate the underlying biogeochemical processes associated with *G. prisca*.

Nitrogen isotopes of *G. prisca*- rich sedimentary rocks, including samples from the Goldwyer Formation, have been reported previously (Kiipli and Kiipli, 2013) which exhibited average $\delta^{15}\text{N}$ values of +7.4‰. Relative to the atmospheric N₂ source (0‰), denitrification in the water column leads to a much larger isotopic fractionation (~20‰) than microbial nitrogen fixation (<3‰) (Luo et al., 2016). These results indicate that denitrification occurred when *G. prisca* was abundant, suggesting *G. prisca* was a nitrate using not N₂-fixing microorganism (Kiipli and Kiipli, 2013). Cyanobacteria and aerobic methanotrophs have the ability to fix atmospheric nitrogen, thus providing a potential nitrogen source for *G. prisca*.

5.4 Significance of microfossils and terrestrial biomarkers

Land-plant input is evident from the presence of cryptospores and, potentially, a trilete spore in Unit 4 of Theia-1 (Fig. 3). Extensive palynological studies have been performed on the Goldwyer Formation (e.g. Quintavalle and Playford, 2008, 2006; Winchester-Seeto et al., 2000; Foster et al., 1986 and references therein) but this is the first study to find probable land-plant spores. Because of the scarcity of records of land-plant spores within the upper Goldwyer Formation, we suggest that the terrestrial palynomorphs found in Theia-1 are locally derived rather than transported from the hinterland. Palaeogeographic maps indicate the presence of peritidal environments on the Broome Platform (Romine et al., 1994) and periodic exposure of these areas would have allowed for the formation and development of terrestrial life.

To date, the earliest uncontroversial record of land plants (embryophytes) is Early-Middle Ordovician (Dapingian) (Rubinstein et al., 2010), predating the Goldwyer Formation. The samples of the present study therefore provide an exceptional opportunity to investigate terrestrial inputs of organic matter during the Ordovician and potentially identify biomarker signals of early land-plants. Middle to Late Ordovician terrestrial organisms and ecosystems most likely comprised microbial mats, bryophytes/bryophyte-like plants and fungi (Redecker et al., 2000; Wellman and Gray, 2000). The fungi and spores identified in this period indicate that soil development was sufficient to support early bryophytes (Redecker et al., 2000). Little is known about terrestrially sourced aliphatic and aromatic biomarker signatures of Ordovician plants (e.g. see Romero-Sarmiento et al., 2011). Most commonly used terrigenous proxies for Upper Paleozoic to recent sediments include long-chain *n*-alkanes derived from plant waxes (Eglinton and Hamilton, 1967), degradation products from conifer resins (e.g. Otto and Simoneit, 2001), and the isotopic composition of plant-derived mid- to long-chain

n-alkanes (Bird et al., 1995; Chikaraishi and Naraoka, 2003; Eley et al., 2016; Naraoka and Ishiwatari, 1999; Rieley et al., 1991).

Modern bryophytes (e.g. *Sphagnum* mosses) and aquatic macrophytes are common sources for mid-chain *n*-alkanes (C_{21} , C_{23} , C_{25}), and their relative abundance can be used to trace macrophytes and/or bryophytes in ancient deposits (e.g. Ficken et al., 2000; Inglis et al., 2015; McKirdy et al., 2010; Mead et al., 2005; Tulipani et al., 2014). Some samples from Santalum-1A had alkane distributions that are dominated by mid-chain *n*-alkanes (Fig. 4b, 4e-f, 8, S5). One of these samples also exhibited a slight OEP at *n*- C_{25} and *n*- C_{27} (Fig. 4b), a typical bryophyte signature (e.g. Inglis et al., 2015). Stable carbon isotopes of *n*- C_{23-32} are more depleted in $\delta^{13}C$ (average of -31.0‰) than *n*- C_{16-19} (average of -27.8‰), suggesting that different sources are contributing to the short-chain and mid-chain *n*-alkanes (Fig. 12, Fig. S5). To further assess the significance of this isotopic discrepancy, the difference in $\delta^{13}C$ between short- and mid-chain *n*-alkanes was calculated (Table 6). These values show that the isotopic shift towards depleted $\delta^{13}C$ is greater in the Santalum-1A samples ($\delta^{13}C(n-C_{16-19}) - \delta^{13}C(n-C_{23-32}) = 2.3$ to 4‰) in comparison to the samples from Solanum-1, Goldwyer-1 and Theia-1 ($\delta^{13}C(n-C_{16-19}) - \delta^{13}C(n-C_{23-32}) = -0.3$ to 1.5‰). Taking into account the geological context and presence of land-plant spores, non-vascular C3 plants (i.e. bryophytes or aquatic macrophytes) are thought to have contributed to the mid-chain *n*-alkanes preserved in the upper Goldwyer Formation at Santalum-1A. Possible explanations for the depleted mid-chain *n*-alkane signature include (i) atmospheric CO_2 may have been depleted which is readily reflected in bryophyte $\delta^{13}C$ as these plants lack stomata to regulate their resistance to inwards CO_2 diffusion (e.g. Royles et al., 2014), or (ii) bryophyte biosynthesis of lipids underlies fractionation of the *n*-alkanes (e.g. Brader et al., 2010). A third possibility may be that bryophytes use recycled and isotopically depleted CO_2 from methanotrophs, which is well known from modern-day environments (Kip et al., 2010; Nichols et al., 2014).

High abundances of benzonaphthofurans were present in the Theia-1 sample from 1217.67–1217.7 m, which also contained the terrestrial palynomorphs. Although the origin of oxygenated heterocyclic aromatic compounds such as dibenzofurans and benzonaphthofurans is still unknown, these compounds prevail in terrestrial sediments and previous studies have suggested a land-plant origin (Li and Ellis, 2015; Sephton et al., 2005; Versteegh and Riboulleau, 2010). In this case, the co-occurrence of benzonaphthofurans with the cryptospores and the absence of these aromatic compounds in other Goldwyer Formation samples points towards a common terrestrial source.

5.5 Regional and global correlations of the Goldwyer Formation

This study investigated palaeoenvironmental conditions associated with the deposition of the Middle Ordovician Goldwyer Formation in the Canning Basin, Western Australia. As no biomarker studies are known from age-equivalent sections elsewhere in the world, little can be said about the (geographical) diversity of biomarkers during the Darriwilian. However, the results of this study can be compared to slightly older and younger Ordovician biomarker studies from Gondwana, Laurentia and Baltica, particularly in relation to *G. prisca* and sterane assemblages. As mentioned in section 5.3, variations in carbon isotopic signatures are observed in *G. prisca* biomass from Australia (Canning and Amadeus Basins) and North America. In the Amadeus Basin, *G. prisca*-rich sediments are present in the Early-Middle Ordovician Horn Valley Siltstone (Elphinstone, 1989). *G. prisca*-rich sediments are also known from the adjacent Georgina Basin, but these are of Cambrian age (e.g. Boreham and Ambrose, 2007). Whether or not the Canning, Amadeus and Georgina Basins were connected at any given time during the Ordovician remains controversial (e.g. Haines and Wingate 2007, Jakobsen et al., 2013). Macrofossil fauna from the Amadeus are highly endemic in comparison to the Canning and Georgina Basin (Jakobsen et al., 2013a, 2013b) and the

Canning and Georgina Basins lack characteristic peri-Gondwanan Ordovician acritarchs (Molyneux et al., 2013). The distinctive nature of the (micro)fauna in the intracratonic Australian basins might suggest limited interaction with the open ocean as oceanic circulation patterns are thought to be reasonably well established during the Middle Ordovician (Servais et al., 2014). Results of this study show some isotopic similarities in *G. prisca* related sediments and oils of the Canning and Amadeus Basins, but further work is required to systematically compare biomarker assemblages and evaluate regional similarities.

Late Ordovician sections from Laurentia and Baltica have been used to study molecular biosignatures preserved in low latitudinal tropical environments (Mustafa et al., 2015; Pancost et al., 2013, 1999, 1998; Rohrssen et al., 2013). The Late Ordovician (Katian–Hirnantian) in eastern Canada (Vauréal Fm. and Ellis Bay Fm.) experienced similarly high bacterial and methanotrophic activity (Rohrssen et al., 2013) as presented here for Unit 4 of the Middle Ordovician Goldwyer Formation. Both the Canadian and Australian sedimentary sections were deposited on tropical carbonate platforms. Hence, elevated bacterial and methanotrophic activity could have been a widespread phenomenon occurring throughout the Middle–Late Ordovician, as carbonate-rich shallow marine environments represented much of the epeiric seas that covered large areas of the landmasses. The sedimentary sections of eastern Canada and the Australian Goldwyer Formation show significant affiliations in chitinozoan assemblages, but this similarity is not mirrored by the associated acritarchs (Quintavalle and Playford, 2006). The Goldwyer Formation contains higher relative abundances of C₃₀ steranes (up to 2.8 %) in comparison to the Ordovician localities from Canada and North America (up to 0.4%; Rohrssen et al., 2015). Differences are also noted in the C₂₇:C₂₈:C₂₉ sterane distribution, with the Canadian sections showing a consistent predominance of C₂₉ steranes (>60%). Furthermore, no *G. prisca* biomarker signatures are present in rock extracts from the Vauréal or Ellis Bay Formation (Rohrssen et al., 2013). Although eastern Canada was situated at low latitudes during the Late Ordovician, sea

surface temperatures are estimated to be more than 5 degrees cooler in comparison to the Dariwillian (Trotter et al., 2008) which may have driven the observed variations in biodiversity, both on the macrofossil and molecular scale.

Further variations are noted in sterane assemblages from other localities in Laurentia and Baltica. In Iowa and Ontario, Middle-Late Ordovician sections exhibit either equal amounts of the C₂₇ and C₂₉ steranes, or a predominance of the C₂₉ steranes (ca. 50-60%) (Pancost et al., 2013; Obermajer et al., 1999). In sections from Baltica, a predominance of C₂₉ steranes is observed during the Katian, which shifts to a strong predominance of C₂₇ steranes (ca. 50-98%) during the Hirnantian (Smolarek et al., 2017; Mustafa et al., 2015). Despite the limited amount of data, these geographical and temporal variations highlight the potential for biomarker studies to evaluate biodiversity changes throughout the Ordovician period.

There is a growing body of evidence that terrestrial life originated on the Gondwanan palaeocontinent during the Early–Middle Ordovician (Stemans et al., 2010 and references therein). Land-plant microfossils have been recorded from the Middle and Upper Ordovician of Gondwana and peri-Gondwana terranes (Argentina, Czech Republic, Saudi Arabia, Libya, Turkey), Avalonia and China (Stemans et al., 2010) (Fig. 13). The microfossil assemblages of Unit 4 represent the oldest land-plant spores from Australia. They are time-equivalent to those found in other Gondwanan localities, contributing to the numerous lines of evidence that terrestrial life originated on Gondwana. Some of these studies detected land-plant spores in similar depositional environments (Strother et al., 2015), but none include published biomarker and compound-specific stable isotope analyses. In this study, the combination of biomarkers and palynology has proven successful to identify terrigenous inputs into the marine environment. Thus, biomarkers provide a powerful tool to track terrestrial signals in Early Palaeozoic settings when microfossils are either scarce or absent.

6 Conclusions

This study investigated the fossil and biomarker signature of Middle Ordovician rocks in the Canning Basin of Australia, which are coeval with the GOBE. Palynological, petrographic, molecular and stable carbon ($\delta^{13}\text{C}$) isotope analyses of biomarkers have demonstrated that the upper (Unit 4) organic-rich section of the Middle Ordovician Goldwyer Formation penetrated on the Broome Platform contains a hitherto unrecognised land plant input. This is the oldest occurrence of land plant microfossils (cryptospores) in Australia, supporting the observation that life on land evolved on the Gondwanan palaeocontinent. Terrestrial biomarkers identified in Unit 4 included benzonaphthofurans and ^{13}C -depleted mid-chain *n*-alkanes.

Molecular redox proxies and hopane and sterane distributions revealed differences between the upper (Unit 4) and lower (Units 1+2) Goldwyer Formation, with the microbial communities changing with the redox conditions. Methanotrophic bacteria were abundant in Unit 4 and similar assemblages were observed in the Upper Ordovician carbonate dominated, shallow marine sediments of Laurentia, suggesting that enhanced methane cycling played an important role in tropical carbonate dominated environments during the Middle–Late Ordovician. In Unit 4 of Solanum-1, the abundance of methanotrophic bacteria correlated with higher inputs of *G. prisca*. The depleted carbon isotopic composition of *G. prisca* biomarkers suggests a potential ecological affiliation where methanotrophic bacteria provided the carbon source for *G. prisca*. The co-occurrence of land plants and methanotrophic bacteria within this setting may also point towards a symbiotic relationship. These findings highlight the ecological significance of methanotrophic bacteria during the Ordovician. *G. prisca* was absent in Units 1+2 but present in Unit 4 at varying abundances. *G. prisca*-rich layers displayed the highest hydrogen indices, signifying the good to excellent petroleum source rock potential associated with this organism. However, these *G. prisca*-rich layers are scarce with a patchy distribution throughout Unit 4 in the wells studied across the Broome

586 Platform, limiting its petroleum source rock potential. New data from Theia-1 indicates that
587 the lower Goldwyer Formation (Units 1+2) has significant source potential, although this is
588 difficult to map due to the paucity of wells.

589 The results of this study provide further insight into Ordovician palaeoenvironmental
590 conditions for both marine- and terrestrial-ecosystems. Combining biomarkers and stable
591 carbon isotopic studies with palynology and organic petrology has enabled the investigation
592 into the biosignatures of early land plants. This combined approach could be applied to
593 additional Ordovician sections where microfossils are scarce, and could assist with the
594 delineation of the geographical distribution and origin of early land plants.

595

Acknowledgements

Geoff Chidlow, Peter Hopper and Alex Holman are thanked for their technical support with GC-MS and GC-irMS analyses at Curtin University. GS acknowledges Curtin University for an International Postgraduate Research Scholarship (CIPRS) and The Institute for Geoscience Research (TIGeR) and CSIRO for top-up scholarships. KG acknowledges the ARC for a DORA (DP130100577) grant to support this research and PhD stipend of GS. DE publishes with the permission of the CEO, Geoscience Australia. GS wishes to thank GSWA and Finder Exploration Pty Ltd for access to drill core and Leon Normore (GSWA) for his assistance with sampling. Furthermore Finder Exploration is thanked for generously providing additional data on Theia-1, including geochemical analyses performed at the Weatherford Labs. Zhongsheng Li is thanked for his contributions to the organic petrology. Carolyn L. K. Colonero assisted with MRM analyses at MIT where research was supported by an award from the Simons Foundation. Chris Elders is acknowledged for his inputs regarding geological interpretations. Chris Boreham and Takehiko (Riko) Hashimoto are thanked for their reviews. Two anonymous reviewers are thanked for their constructive and useful comments.

References

- Bird, M.I., Summons, R.E., Gagan, M.K., Roksandic, Z., Dowling, L., Head, J., Fifield, L.K., Cresswell, R.G., Johnson, D.P., 1995. Terrestrial vegetation change inferred from *n*-alkane $\delta^{13}\text{C}$ analysis in the marine environment. *Geochimica et Cosmochimica Acta* 59, 2853–2857.
- Blokker, P., van Bergen, P., Pancost, R., Collinson, M.E., de Leeuw, J.W., Sinninghe Damsté, J.S., 2001. The chemical structure of *Gloeocapsomorpha prisca* microfossils: Implications for their origin. *Geochimica et Cosmochimica Acta* 65, 885–900.
- Boreham, C.J., Ambrose, G.J., 2007. Cambrian petroleum systems in the southern Georgina Basin, Northern Territory, Australia., in: Munson, T.J., Ambrose, G.J. (Eds),

622 Proceedings of the Central Australian Basins Symposium (CABS), Alice Springs,
 623 Northern Territory, Northern Territory Geological Survey Special Publication 2.
 624 Brader, A. V., van Winden, J.F., Bohncke, S.J.P., Beets, C.J., Reichart, G., de Leeuw, J.W.,
 625 2010. Fractionation of hydrogen , oxygen and carbon isotopes in *n*-alkanes and cellulose
 626 of three Sphagnum species. Organic Geochemistry 41, 1277–1284.
 627 doi:10.1016/j.orggeochem.2010.09.006
 628 Brocks, J.J., Summons, R.E., 2014. Sedimentary hydrocarbons, biomarkers for early life, in:
 629 Holland, H., Turekian, K. (Eds.), Treatise on Geochemistry 2nd Edition. Elsevier, pp.
 630 63–115. doi:10.1016/B978-0-08-095975-7.00803-2
 631 Brocks, J.J., Buick, R., Logan, G.A., Summons, R.E., 2003. Composition and syngeneity of
 632 molecular fossils from the 2.78 to 2.45 billion-year-old Mount Bruce Supergroup,
 633 Pilbara Craton, Western Australia. Geochimica et Cosmochimica Acta 67, 22, 4289–
 634 4319.
 635 Chikaraishi, Y., Naraoka, H., 2003. Compound-specific $\delta D - \delta^{13}C$ analyses of *n*-alkanes
 636 extracted from terrestrial and aquatic plants. Phytochemistry 63, 361–371.
 637 doi:10.1016/S0031-9422(02)00749-5
 638 Cooper, R.A., Sadler, P.M., 2004. The Ordovician Period, in: A Geologic Time Scale. pp.
 639 165–187.
 640 Didyk, B.M., Simoneit, B.R.T., Brassell, S.C., Eglinton, G., 1978. Organic geochemical
 641 indicators of palaeoenvironmental conditions of sedimentation. Nature 272, 216–222.
 642 doi:10.1038/272216a0
 643 Dutta, S., Brocke, R., Hartkopf-Fröder, C., Littke, R., Wilkes, H., Mann, U., 2007. Highly
 644 aromatic character of biogeomacromolecules in Chitinozoa: A spectroscopic and
 645 pyrolytic study. Organic Geochemistry 38, 1625–1642.
 646 doi:10.1016/j.orggeochem.2007.06.014
 647 Edwards, D., Morris, J.L., Richardson, J.B., Kendrick, P., 2014. Cryptospores and

cryptophytes reveal hidden diversity in early land floras. *New Phytologist* 202: 50–78.
doi: 10.1111/nph.12645

Edwards, D.S., Boreham, C.J., Chen, J., Grosjean, E., Mory, A.J., Sohn, J., Zumberge, J.E.,
2013. Stable carbon and hydrogen isotopic compositions of Paleozoic marine crude oils
from the Canning Basin: comparison with other west Australian crude oils, in: Keep, M.
and Moss, S. (Eds), *The Sedimentary Basins of West Australia IV. Proceedings of the
Petroleum Exploration Society of Australia Symposium, Perth, 2013*, pp. 1–13.

Edwards, D.S., Zumberge, J.E., 2005. *The Oils of Western Australia. II. Regional Petroleum
Geochemistry and Correlation of Crude Oils and Condensates from Western Australia
and Papua New Guinea*, Geoscience Australia and GeoMark Research Ltd unpublished
report, Canberra and Houston, GEOCAT 37512, [http://www.ga.gov.au/metadata-
gateway/metadata/record/gcat_a05f7892-cafb-7506-e044-
00144fdd4fa6/The+Oils+of+Western+Australia+II](http://www.ga.gov.au/metadata-gateway/metadata/record/gcat_a05f7892-cafb-7506-e044-00144fdd4fa6/The+Oils+of+Western+Australia+II).

Edwards, D.S., Summons, R.E., Kennard, J.M., Nicoll, R.S., Bradshaw, J., Bradshaw, M.T.,
Foster, C.B., O'Brien, G.W., Zumberge, J.E., 1997. Geochemical characteristics of
Palaeozoic petroleum systems in northwestern Australia. *APPEA Journal* 37(1), 351–
379. doi:10.1007/PL00007202

Edwards, D.S., Murray, A.P., Foster, C.B., 1995. *Hydrocarbon Composition of Carribuddy
Group Sediments, Oils and Bitumens from the Admiral Bay Fault Zone, Canning Basin*.
Australian Geological Survey Organisation, 31p.

Eglinton, G., Hamilton, R.J., 1967. Leaf epicuticular waxes. *Science* 156, 1322–1335.

Eley, Y., Dawson, L., Pedentchouk, N., 2016. Investigating the carbon isotope composition
and leaf wax n-alkane concentration of C3 and C4 plants in Stiffkey saltmarsh, Norfolk,
UK. *Organic Geochemistry* 96, 28–42. doi:10.1016/j.orggeochem.2016.03.005

Elphinstone R., 1989. *Sedimentology and facies distribution within the Horn Valley
Siltstone, Amadeus Basin: A reconnaissance study*. Bureau of Mineral Resources,

674 Australia, Record 1992/02.

675 Farrimond, P., Talbot, H.M., Watson, D.F., Schulz, L.K., Wilhelms, A., 2004.

676 Methylhopanoids: molecular indicators of ancient bacteria and a petroleum correlation

677 tool. *Geochimica et Cosmochimica Acta* 68, 3873–3882. doi:10.1016/j.gca.2004.04.011

678 Ficken, K.J., Li, B., Swain, D.L., Eglinton, G., 2000. An n-alkane proxy for the sedimentary

679 input of submerged/floating freshwater aquatic macrophytes. *Organic Geochemistry* 31,

680 745–749. doi:10.1016/S0146-6380(00)00081-4

681 Finder Exploration Pty Ltd, 2015. Theia 1 Rig Release and Cessation of Operations, 31

682 August 2015. [http://www.finderexp.com/wp-](http://www.finderexp.com/wp-content/uploads/2015/08/Cessation%20of%20operations%20at%20Theia-1%2031%20Aug%2015.pdf)

683 [content/uploads/2015/08/Cessation%20of%20operations%20at%20Theia-](http://www.finderexp.com/wp-content/uploads/2015/08/Cessation%20of%20operations%20at%20Theia-1%2031%20Aug%2015.pdf)

684 [1%2031%20Aug%2015.pdf](http://www.finderexp.com/wp-content/uploads/2015/08/Cessation%20of%20operations%20at%20Theia-1%2031%20Aug%2015.pdf).

685 Forman, D.J., Wales, D.W., 1981. Geological evolution of the Canning Basin, Western

686 Australia. *Bureau of Mineral Resources Bulletin* 210, 1–390.

687 Foster, C.B., O'Brien, G.W., Watson, S.T., 1986. Hydrocarbon source potential of the

688 Goldwyer Formation, Barbwire Terrace, Canning Basin, Western Australia. *APEA*

689 *Journal* 26, 142–155.

690 Foster, C., Reed, J., Wicander, R., 1989. *Gloeocapsomorpha prisca* Zalesky 1917: A New

691 Study Part 1: Taxonomy, Geochemistry and Paleoecology. *Geobios* 22, 735–759.

692 Foster, C.B., Wicander, R., Reed, J., 1990. *Gloeocapsomorpha prisca* Zalesky, 1917: A

693 New Study Part II: origin of kukersite, a new interpretation. *Geobios* 23, 133–140.

694 Fowler, M.G., Stasiuk, L.D., Hearn, M., Obermajer, M., 2004. Evidence for

695 *Gloeocapsomorpha prisca* in Late Devonian source rocks from Southern Alberta,

696 Canada. *Organic Geochemistry* 35, 425–441. doi:10.1016/j.orggeochem.2004.01.017

697 Gill, B.C., Lyons, T.W., Saltzman, M.R., 2007. Parallel, high-resolution carbon and sulfur

698 isotope records of the evolving Paleozoic marine sulfur reservoir. *Palaeogeography,*

699 *Palaeoclimatology, Palaeoecology* 256, 156–173. doi:10.1016/j.palaeo.2007.02.030

700 Grantham, P.J., Wakefield, L.L., 1988. Variations in the sterane carbon number distributions
701 of marine source rock derived crude oils through geological time. *Organic Geochemistry*
702 12, 1, 61–73.

703 Grice, K., Schaeffer, P., Schwark, L., Maxwell, J.R., 1996. Molecular indicators of
704 palaeoenvironmental conditions in an immature Permian shale (Kupferschiefer, Lower
705 Rhine Basin, north-west Germany) from free and S-bound lipids. *Organic Geochemistry*
706 25, 3/4, 131–147.

707 Grice, K., Cao, C., Love, G.D., Bottcher, M.E., Twitchett, R., Grosjean, E., Summons, R.E.,
708 Turgeon, S.E., Dunning, W., Jin, Y., 2005. Photic zone euxinia during the Permian-
709 Triassic superanoxic event. *Science* 307, 706–709.

710 Grosjean, E., Love, G.D., Stalvies, C., Fike, D.A., Summons, R.E., 2009. Origin of petroleum
711 in the Neoproterozoic-Cambrian South Oman Salt Basin. *Organic Geochemistry* 40, 87–
712 110. doi:10.1016/j.orggeochem.2008.09.011

713 Gupta, N.S., Briggs, D.E., Pancost, R.E., 2006. Molecular taphonomy of graptolites. *Journal*
714 *of the Geological Society London* 163, 897–900.

715 Guthrie, J.M., Pratt, L.M., 1995. Geochemical character and origin of oils in Ordovician
716 reservoir rocks, Illinois and Indiana, USA. *American Association of Petroleum*
717 *Geologists Bulletin* 79, 1631–1649. doi:10.1306/7834DE36-1721-11D7-
718 8645000102C1865D

719 Haines, P.W., Wingate, M.T.D., 2007. Contrasting depositional histories, detrital zircon
720 provenance and hydrocarbon systems: Did the Larapintine Seaway link the Canning and
721 Amadeus Basin during the Ordovician? *Proceedings Central Australian Basin*
722 *Symposium, Special Publications* 2, 36–51.

723 Haines, P.W., 2004. Depositional facies and regional correlation for the Ordovician
724 Goldwyer and Nita formations Canning Basin, Western Australia with implications for
725 petroleum exploration: Western Australia Geological Survey, Record 2004/7, 45p.

726 Hammarlund, E.U., Dahl, T.W., Harper, D.A.T., Bond, D.P.G., Nielsen, A.T., Bjerrum, C.J.,
 727 Schovsbo, N.H., Schönlaub, H.P., Zalasiewicz, J. a., Canfield, D.E., 2012. A sulfidic
 728 driver for the end-Ordovician mass extinction. *Earth and Planetary Science Letters* 331–
 729 332, 128–139. doi:10.1016/j.epsl.2012.02.024
 730 Harper, D.A.T., 2006. The Ordovician biodiversification: setting an agenda for marine life.
 731 *Palaeogeography, Palaeoclimatology, Palaeoecology* 232, 148–166.
 732 doi:10.1016/j.palaeo.2005.07.010
 733 Hoffmann, C.F., Foster, C.B., Powell, T.G., Summons, R.E., 1987. Hydrocarbon biomarkers
 734 from Ordovician sediments and the fossil alga *Gloeocapsomorpha prisca* Zalesky
 735 1917. *Geochimica et Cosmochimica Acta* 51, 2681–2697. doi:10.1016/0016-
 736 7037(87)90149-9
 737 Hughes, W.B., Holba, A.G., Dzou, L.I.P., 1995. The ratios of dibenzothiophene to
 738 phenanthrene and pristane to phytane as indicators of depositional environment and
 739 lithology of petroleum source rocks. *Geochimica et Cosmochimica Acta* 59, 3581–3598.
 740 doi:10.1016/0016-7037(95)00225-O
 741 Inglis, G.N., Collinson, M.E., Riegel, W., Wilde, V., Robson, B.E., Lenz, O.K., Pancost,
 742 R.D., 2015. Ecological and biogeochemical change in an early Paleogene peat-forming
 743 environment: linking biomarkers and palynology. *Palaeogeography, Palaeoclimatology,*
 744 *Palaeoecology* 438, 245–255. doi:10.1016/j.palaeo.2015.08.001
 745 Jacob, J., Paris, F., Monod, O., Miller, M.A., Tang, P., George, S.C., Bény, J., 2007. New
 746 insights into the chemical composition of chitinozoans. *Organic Geochemistry* 38,
 747 1782–1788.
 748 Jarrett, A., Edwards, D.S., Boreham, C., McKirdy, D.M., 2016. Petroleum Geochemistry of
 749 the Amadeus Basin. AGES 2016 Conference Proceedings, NT Geological Survey.
 750 Kennard, J.M., Jackson, M.J., Romine, K.K., Shaw, R.D., Southgate, P.N., 1994.
 751 Depositional sequences and associated petroleum systems of the Canning Basin, WA,

752 in: The Sedimentary Basins of Western Australia. Proceedings of the Petroleum
 753 Exploration Society of Australia Symposium, Perth, WA, pp. 658–676.
 754 Kiipli, E., Kiipli, T., 2013. Nitrogen isotopes in kukersite and black shale implying
 755 Ordovician-Silurian seawater redox conditions. *Oil Shale* 30, 60–75.
 756 doi:10.3176/oil.2013.1.06
 757 Kip, N., van Winden, J.F., Pan, Y., Bodrossy, L., Reichart, G.-J., Smolders, A.J.P., Jetten,
 758 M.S.M., Sinninghe Damsté, J.S., Op den Camp, H.J.M., 2010. Global prevalence of
 759 methane oxidation by symbiotic bacteria in peat-moss ecosystems. *Nature Geoscience* 3,
 760 617–621. doi:10.1038/ngeo939
 761 Koopmans, M.P., Köster, J., van Kaam-Peters, H.M.E., Kenig, F., Schouten, S., Hartgers,
 762 W.A., De Leeuw, J.W., Sinninghe Damsté, J.S., 1996. Diagenetic and catagenetic
 763 products of isorenieratene: molecular indicators for photic zone anoxia. *Geochimica et*
 764 *Cosmochimica Acta* 60, 4467–4496. doi:10.1016/S0016-7037(96)00238-4
 765 LaPorte, D.F., Holmden, C., Patterson, W.P., Loxton, J.D., Melchin, M.J., Mitchell, C.E.,
 766 Finney, S.C., Sheets, H.D., 2009. Local and global perspectives on carbon and nitrogen
 767 cycling during the Hirnantian glaciation. *Palaeogeography, Palaeoclimatology,*
 768 *Palaeoecology* 276, 182–195. doi:10.1016/j.palaeo.2009.03.009
 769 Le Heron, D.P., Craig, J., Etienne, J.L., 2009. Ancient glaciations and hydrocarbon
 770 accumulations in North Africa and the Middle East. *Earth-Science Reviews* 93, 47–76.
 771 doi:10.1016/j.earscirev.2009.02.001
 772 Lenton, T.M., Crouch, M., Johnson, M., Pires, N., Dolan, L., 2012. First plants cooled the
 773 Ordovician. *Nature Geoscience* 5, 86–89. doi:10.1038/ngeo1390
 774 Lenton, T.M., Dahl, T.W., Daines, S.J., Mills, B.J.W., Ozaki, K., Saltzman, M.R., Porada, P.,
 775 2016. Earliest land plants created modern levels of atmospheric oxygen. *Proceedings of*
 776 *the National Academy of Sciences* 113, 9704–9709. doi:10.1073/pnas.1604787113
 777 Li, M., Ellis, G.S., 2015. Qualitative and quantitative analysis of dibenzofuran,

778 alkyldibenzofurans, and benzo[*b*]naphthofurans in crude oils and source rock extracts.
 779 Energy & Fuels 29, 1421–1430. doi:10.1021/ef502558a
 780 Luo, G., Algeo, T.J., Zhan, R., Yan, D., Huang, J., Liu, J., Xie, S., 2016. Perturbation of the
 781 marine nitrogen cycle during the Late Ordovician glaciation and mass extinction.
 782 Palaeogeography, Palaeoclimatology, Palaeoecology 448, 339–348.
 783 doi:10.1016/j.palaeo.2015.07.018
 784 McKirdy, D.M., Thorpe, C.S., Haynes, D.E., Grice, K., Krull, E.S., Halverson, G.P.,
 785 Webster, L.J., 2010. The biogeochemical evolution of the Coorong during the mid- to
 786 late Holocene: an elemental, isotopic and biomarker perspective. Organic Geochemistry
 787 41, 96–110. doi:10.1016/j.orggeochem.2009.07.010
 788 Mead, R., Xu, Y., Chong, J., Jaffle, R., 2005. Sediment and soil organic matter source
 789 assessment as revealed by the molecular distribution and carbon isotopic composition of
 790 *n*-alkanes. Organic Geochemistry 36, 363–370.
 791 Melchin, M.J., Mitchell, C.E., Holmden, C., Štorch, P., 2013. Environmental changes in the
 792 Late Ordovician – early Silurian : review and new insights from black shales and
 793 nitrogen isotopes. GSA Bulletin 125, 1635–1670. doi:10.1130/B30812.1
 794 Moldowan, J.M., Seifert, W.K., Gallegos, E.J., 1985. Relationship between petroleum
 795 composition and depositional environment of petroleum source rocks. The American
 796 Association of Petroleum Geologists Bulletin 69, 191–207.
 797 doi:10.1080/00167638508949779
 798 Moldowan, J.M., Fago, F.J., Lee, C.Y., Jacobson, S.R., Watt, D.S., Slougui, N., Jeganathan,
 799 A., Young, D.C., 1990. Sedimentary 24-*n*-propylcholestanes, molecular fossils
 800 diagnostic of marine algae. Science 247, 309–312.
 801 Munnecke, A., Calner, M., Harper, D. a T., Servais, T., 2010. Ordovician and Silurian sea-
 802 water chemistry, sea level, and climate: a synopsis. Palaeogeography,
 803 Palaeoclimatology, Palaeoecology 296, 389–413. doi:10.1016/j.palaeo.2010.08.001

804 Mustafa, K.A., Sephton, M.A., Watson, J.S., Spathopoulos, F., Krzywiec, P., 2015. Organic
805 geochemical characteristics of black shales across the Ordovician-Silurian boundary in
806 the Holy Cross Mountains, central Poland. *Marine and Petroleum Geology* 66, 1042–
807 1055. doi:10.1016/j.marpetgeo.2015.08.018

808 Naraoka, H., Ishiwatari, R., 1999. Carbon isotopic compositions of individual long-chain *n*-
809 fatty acids and n-alkanes from river to open ocean: multiple origins for their occurrence.
810 *Geochemical Journal* 33, 215–235.

811 Nichols, J.E., Isles, P.D.F., Peteet, D.M., 2014. A novel framework for quantifying past
812 methane recycling by *Sphagnum*-methanotroph symbiosis using carbon and hydrogen
813 isotope ratios of leaf wax biomarkers. *Geochemistry, Geophysics, Geosystems* 15,
814 1827–1836. doi:10.1002/2014GC005242

815 Obermajer, M., Fowler, M.G., Snowdon, L.R., 1999. Depositional environment and oil
816 generation in Ordovician source rocks from southwestern Ontario, Canada: Organic
817 geochemical and petrological approach. *AAPG Bulletin* 83, 1426–1453.
818 doi:10.1306/E4FD41D9-1732-11D7-8645000102C1865D

819 Otto, A., Simoneit, B.R.T., 2001. Chemosystematics and diagenesis of terpenoids in fossil
820 conifer species and sediment from the Eocene Zeitz Formation, Saxony, Germany.
821 *Geochimica et Cosmochimica Acta* 65, 3505–3527. doi:10.1016/S0016-7037(01)00693-
822 7

823 Pancost, R.D., Freeman, K.H., Herrmann, A.D., Patzkowsky, M.E., Ainsaar, L., Martma, T.,
824 2013. Reconstructing Late Ordovician carbon cycle variations. *Geochimica et*
825 *Cosmochimica Acta* 105, 433–454. doi:10.1016/j.gca.2012.11.033

826 Pancost, R.D., Freeman, K.H., Patzkowsky, M.E., 1999. Organic-matter source variation and
827 the expression of a late Middle Ordovician carbon isotope excursion. *Geology* 27, 1015–
828 1018. doi:10.1130/0091-7613(1999)027<1015:OMSVAT>2.3.CO

829 Pancost, R.D., Freeman, K.H., Patzkowsky, M.E., Wavrek, D.A., Collister, J.W., 1998.

830 Molecular indicators of redox and marine photoautotroph composition in the late Middle
831 Ordovician of Iowa, U.S.A. *Organic Geochemistry* 29, 1649–1662. doi:10.1016/S0146-
832 6380(98)00185-5

833 Peters, K.E., Walters, C.C., Moldowan, J.M., 2005. *The Biomarker Guide Volume 2.*
834 *Biomarkers and Isotopes in Petroleum Systems and Earth History*, 2nd ed. Cambridge
835 University Press.

836 Quintavalle, M., Playford, G., 2008. Stratigraphic distribution of selected acritarchs in the
837 Ordovician subsurface, Canning Basin, Western Australia. *Revue de micropaléontologie*
838 51, 23-37. doi:10.1016/j.revmic.2006.11.003

839 Quintavalle, M., Playford, G., 2006. Palynostratigraphy of Ordovician strata, Canning Basin,
840 Western Australia. Part Two: chitinozoans and biostratigraphy. *Palaeontographica*
841 Abteilung B: 275(4-6), 89-131.

842 Redecker, D., Kodner, R., Graham, L.E., 2000. Glomalean fungi from the Ordovician.
843 *Science* 289, 1920–1921.

844 Reed, J.D., Illich, H.A., Horsfield, B., 1986. Biochemical evolutionary significance of
845 Ordovician oils and their sources. *Organic Geochemistry* 10, 347–358.
846 doi:10.1016/0146-6380(86)90035-5

847 Ricci, J.N., Michel, A.J., Newman, K., 2015. Phylogenetic analysis of HpnP reveals the
848 origin of 2-methylhopanoid production in Alphaproteobacteria. *Geobiology* 13, 267–
849 277.

850 Ricci, J.N., Coleman, M.L., Welander, P. V, Sessions, A.L., Summons, R.E., Spear, J.R.,
851 Newman, D.K., 2014. Diverse capacity for 2-methylhopanoid production correlates with
852 a specific ecological niche. *International Society for Microbial Ecology* 8, 675–684.
853 doi:10.1038/ismej.2013.191

854 Rieley, G., Collier, R.J., Jones, D.M., Eglinton, G., Eakin, P.A., Fallick, A.E., 1991. Sources
855 of sedimentary lipids deduced from stable carbon-isotope analyses of individual

856 compounds. *Nature* 352, 425–427.

857 Rohrssen, M., Gill, B.C., Love, G.D., 2015. Scarcity of the C₃₀ sterane biomarker, 24-*n*-
858 propylcholestane, in Lower Paleozoic marine paleoenvironments. *Organic Geochemistry*
859 80, 1-7. doi:10.1016/j.orggeochem.2014.11.008

860 Rohrssen, M., Love, G.D., Fischer, W., Finnegan, S., Fike, D.A., 2013. Lipid biomarkers
861 record fundamental changes in the microbial community structure of tropical seas during
862 the Late Ordovician Hirnantian glaciation. *Geology* 41, 127–130. doi:10.1130/G33671.1

863 Romero-Sarmiento, M.F., Riboulleau, A., Vecoli, M., Versteegh, G.J.M., 2011. Aliphatic and
864 aromatic biomarkers from Gondwanan sediments of Late Ordovician to Early Devonian
865 age: an early terrestrialization approach. *Organic Geochemistry* 42, 605–617.
866 doi:10.1016/j.orggeochem.2011.04.005

867 Romine, K.K., Southgate, P.N., Kennard, J.M., Jackson, M.J., 1994. The Ordovician to
868 Silurian phase of the Canning Basin WA: structure and sequence evolution, in: Purcell,
869 P.G. and Purcell, R.R. (Eds), *The Sedimentary Basins of Western Australia*. Proceedings
870 of the Petroleum Exploration Society of Australia Symposium, Perth, 1994, pp. 677–
871 696.

872 Royles, J., Horwath, A.B., Griffiths, H., 2014. Interpreting bryophyte stable carbon isotope
873 composition: Plants as temporal and spatial climate recorders. *Geochemistry,*
874 *Geophysics, Geosystems* 15, 1462–1475. doi:10.1002/2013GC005169. Received

875 Rubinstein, C. V., Gerrienne, P., de la Puente, G.S., Astini, R.A., Steemans, P., 2010. Early
876 Middle Ordovician evidence for land plants in Argentina (eastern Gondwana). *New*
877 *Phytologist* 188, 365–369. doi:10.1111/j.1469-8137.2010.03433.x

878 Schwark, L., Empt, P., 2006. Sterane biomarkers as indicators of palaeozoic algal evolution
879 and extinction events. *Palaeogeography, Palaeoclimatology, Palaeoecology* 240, 225–
880 236.

881 Schwark, L., Frimmel, A., 2004. Chemostratigraphy of the Posidonia Black Shale, SW-

882 Germany II. Assessment of extent and persistence of photic-zone anoxia using aryl
 883 isoprenoid distributions, *Chemical Geology* 206, 231–248.
 884 doi:10.1016/j.chemgeo.2003.12.008
 885 Sephton, M.A., van Looy, C., Brinkhuis, H., Wignall, P.B., de Leeuw, J., Visscher, H., 2005.
 886 Catastrophic soil erosion during the end-Permian biotic crisis. *Geology* 33, 941–944.
 887 doi:10.1130/G21784.1
 888 Servais, T., Harper, D.A.T., Li, J., Munnecke, A., Owen, A.W., Sheehan, P.M., 2009.
 889 Understanding the Great Ordovician Biodiversification Event (GOBE): Influences of
 890 paleogeography, paleoclimate, or paleoecology? *GSA Today* 19, 4–10.
 891 doi:10.1130/GSATG37A.1
 892 Servais, T., Li, J., Molyneux, S., Raevskaya, E., 2003. Ordovician organic-walled
 893 microphytoplankton (acritarch) distribution: the global scenario. *Palaeogeography,*
 894 *Palaeoclimatology, Palaeoecology* 195, 149–172. doi:10.1016/S0031-0182(03)00306-7
 895 Sherwood, N., Li, Z., 2016. Source rock evaluation using vitrinite reflectance and maceral
 896 analyses for a suite of rocks sampled from various wells drilled in the Canning Basin,
 897 Western Australia and the Amadeus Basin, Northern Territory, Australia. *Geoscience*
 898 *Australia, Resources Division Report* 2016/00.
 899 Sinninghe Damsté, J.S., Kenig, F., Koopmans, M.P., Koster, J., Schouten, S., Hayes, J.M., de
 900 Leeuw, J.W., 1995. Evidence for gammacerane as an indicator of water column
 901 stratification. *Geochimica et Cosmochimica Acta* 59, 1895–1900. doi:10.1016/0016-
 902 7037(95)00073-9
 903 Smolarek, J., Marynowski, L., Trela, W., Kujawski, P., Simoneit, B. 2017. Redox conditions
 904 and marine microbial community changes during the end-Ordovician mass extinction
 905 event. *Global and Planetary Change* 149, 105–122.
 906 <http://dx.doi.org/10.1016/j.gloplacha.2017.01.002>
 907 Steemans, P., Hérissé, A. Le, Melvin, J., Miller, M.A., Paris, F., Verniers, J., Wellman, C.H.,

908 2009. Origin and radiation of the earliest vascular land plants. *Science* 324, 353.
 909 doi:10.1126/science.1169659

910 Steemans, P., Wellman, C.H., Gerrienne, P., 2010. Palaeogeographic and palaeoclimatic
 911 considerations based on Ordovician to Lochkovian vegetation. Geological Society
 912 London Special Publications 339, 49–58. doi:10.1144/SP339.5

913 Strother, P.K., Traverse, A., Vecoli, M., 2015. Cryptospores from the Hanadir Shale Member
 914 of the Qasim Formation, Ordovician (Darriwilian) of Saudi Arabia: taxonomy and
 915 systematics. *Review of Palaeobotany and Palynology* 212, 97–110.
 916 doi:10.1016/j.revpalbo.2014.08.018

917 Summons, R.E., Bradley, A.S., Jahnke, L.L., Waldbauer, J.R., 2006. Steroids, Triterpenoids
 918 and molecular oxygen. *Philosophical Transactions of the Royal Society B: Biological*
 919 *Sciences* 361, 951–968. doi:10.1098/rstb.2006.1837

920 Summons, R.E., Jahnke, L.L., 1990. Identification of the methylhopanes in sediments and
 921 petroleum. *Geochimica et Cosmochimica Acta* 54, 247–251. doi:10.1016/0016-
 922 7037(90)90212-4

923 Summons, R.E., Jahnke, L.L., Hope, J.M., Logan, G. A, 1999. 2-Methylhopanoids as
 924 biomarkers for cyanobacterial oxygenic photosynthesis. *Nature* 400, 554–557.
 925 doi:10.1038/23005

926 Summons, R.E., Jahnke, L.L., Roksandic, Z., 1994. Carbon isotopic fractionation in lipids
 927 from methanotrophic bacteria: relevance for interpretation of the geochemical record of
 928 biomarkers. *Geochimica et Cosmochimica Acta* 58, 2853–2863. doi:10.1016/0016-
 929 7037(94)90119-8

930 Summons, R.E., Powell, T.G., 1987. Identification of aryl isoprenoids in source rocks and
 931 crude oils: Biological markers for the green sulphur bacteria. *Geochimica et*
 932 *Cosmochimica Acta* 51, 557–566.

933 Talyzina, N.M., Moldowan, J.M., Johannisson, A., Fago, F.J., 2000. Affinities of Early

934 Cambrian acritarchs studied by using microscopy, fluorescence flow cytometry and
 935 biomarkers. *Review of Palaeobotany and Palynology* 108, 37–53. doi:10.1016/S0034-
 936 6667(99)00032-9

937 Thompson, C.K., Kah, L.C., 2012. Sulfur isotope evidence for widespread euxinia and a
 938 fluctuating oxycline in Early to Middle Ordovician greenhouse oceans.
 939 *Palaeogeography, Palaeoclimatology, Palaeoecology* 313–314, 189–214.
 940 doi:10.1016/j.palaeo.2011.10.020

941 Trabucho-Alexandre, J., Hay, W.W., de Boer, P.L., 2011. Phanerozoic environments of black
 942 shale deposition and the Wilson Cycle. *Solid Earth Discussions* 3, 743–768.
 943 doi:10.5194/se-3-29-2012

944 Triche, N.E., Bahar, M., 2013. Shale gas volumetrics of unconventional resource plays in the
 945 Canning Basin, Western Australia, in: *SPE Unconventional Resources Conference and*
 946 *Exhibition Asia Pacific*, Brisbane, Australia, 11–13 November 2013.

947 Tulipani, S., Grice, K., Greenwood, P.F., Haines, P.W., Sauer, P.E., Schimmelmann, A.,
 948 Summons, R.E., Foster, C.B., Böttcher, M.E., Playton, T., Schwark, L., 2015a. Changes
 949 of palaeoenvironmental conditions recorded in Late Devonian reef systems from the
 950 Canning Basin, Western Australia: A biomarker and stable isotope approach. *Gondwana*
 951 *Research* 28, 1500–1515. doi:10.1016/j.gr.2014.10.003

952 Tulipani, S., Grice, K., Greenwood, P.F., Schwark, L., Böttcher, M.E., Summons, R.E.,
 953 Foster, C.B., 2015b. Molecular proxies as indicators of freshwater incursion-driven
 954 salinity stratification. *Chemical Geology* 409, 61–68.
 955 doi:10.1016/j.chemgeo.2015.05.009

956 Tulipani, S., Grice, K., Krull, E., Greenwood, P., Revill, A.T., 2014. Salinity variations in the
 957 northern Coorong Lagoon, South Australia: significant changes in the ecosystem
 958 following human alteration to the natural water regime. *Organic Geochemistry* 75, 74–
 959 86. doi:10.1016/j.orggeochem.2014.04.013

960 van Aarssen, B.G.K., Alexander, R., Kagi, R.I., 2000. Higher plant biomarkers reflect
 961 palaeovegetation changes during Jurassic times. *Geochimica et Cosmochimica Acta* 64,
 962 1417–1424.

963 Vandenbroucke, T.R.A., Armstrong, H.A., Williams, M., Zalasiewicz, J.A., Sabbe, K., 2009.
 964 Ground-truthing Late Ordovician climate models using the paleobiogeography of
 965 graptolites. *Paleoceanography* 24, 1–19. doi:10.1029/2008PA001720

966 Versteegh, G.J.M., Riboulleau, A., 2010. An organic geochemical perspective on
 967 terrestrialization. *Geological Society London Special Publications* 339, 11–36.
 968 doi:10.1144/SP339.3

969 Volkman, J.K., 2006. Lipid markers for marine organic matter, in: *Handbook of*
 970 *Environmental Chemistry, Volume 2: Reactions and Processes*. pp. 27–70.
 971 doi:10.1007/698_2_002

972 Volkman, J.K., 1986. A review of sterol markers for marine and terrigenous organic matter.
 973 *Organic Geochemistry* 9, 83–99. doi:10.1016/0146-6380(86)90089-6

974 Wang, S., Liu, S., Lin, Z., Li, R., Wang, X., Zhou, C., Lou, H., Wang, S., Liu, S., Lin, Z., Li,
 975 R., Wang, X., 2013. Terpenoids from the Chinese liverwort *Plagiochila pulcherrima*
 976 and their cytotoxic effects. *Journal of Asian Natural Products Research* 15, 473–481.
 977 doi:10.1080/10286020.2013.785529

978 Welander, P. V., Summons, R.E., 2012. Discovery, taxonomic distribution, and phenotypic
 979 characterization of a gene required for 3-methylhopanoid production. *Proceedings of the*
 980 *National Academy of Sciences* 109, 12905–12910. doi:10.1073/pnas.1208255109

981 Wellman, C.H., Gray, J., 2000. The microfossil record of early land plants. *Philosophical*
 982 *Transactions of the Royal Society B: Biological Sciences* 355, 717–732.

983 Winchester-Seeto, T., Foster, C., O’Leary, T., 2000. Chitinozoans from the Middle
 984 Ordovician (Darriwilian) Goldwyer and Nita formations, Canning Basin (Western
 985 Australia). *Acta Palaeontologica Polonica* 45, 271–300.

986 Wright, N., Zahirovic, S., Müller, R.D., Seton, M., 2013. Towards community-driven
987 paleogeographic reconstructions: integrating open-access paleogeographic and
988 paleobiology data with plate tectonics. *Biogeosciences* 10, 1529-1541. doi:10.5194/bg-
989 10-1529-2013
990

Captions of tables and figures

Table 1: Summary of palynomorph assemblages and key species identified in this study in the Goldwyer Formation in Goldwyer-1, Santalum1A, Solanum-1 and Theia-1.

Table 2: Summary of Rock-Eval pyrolysis, biomarker and organic petrological data for Units 1+2 and Unit 4 of the Goldwyer Formation in Goldwyer-1, Solanum-1, Santalum-1A and Theia-1.

Table 3: Key aliphatic and aromatic hydrocarbon signatures identified in samples from the Goldwyer Formation and their paleobiological and/or environmental interpretation. *n*-Alkane carbon isotopic values are interpreted to signify different source inputs to Unit 4 at Solanum-1 and Santalum-1A.

Table 4: Key aliphatic and aromatic biomarker parameters for Units 1+2 and Unit 4 of the Goldwyer Formation in Goldwyer-1, Solanum-1, Santalum-1A and Theia-1.

Table 5: *n*-Alkane-specific $\delta^{13}\text{C}$ values [‰ VPDB] for samples from Units 1+2 and Unit 4 of the Goldwyer Formation in selected Canning Basin wells. Reported values represent average values of two or more measurements where the difference between the measurements was equal to, or less than, 0.5 per mil. Where there is no value, the peaks were too small to be measured reliably.

Table 6: Average $\delta^{13}\text{C}$ values for short- (C_{16} - C_{19}) and mid to long- (C_{23} - C_{32}) chain *n*-alkanes in samples from the Goldwyer Formation. The *n*-alkanes show a progressive depletion with increasing carbon number, but the depletion is notably greater in Santalum-1A (Δ) in comparison to other samples.

Figure 1: Well location map and well-well correlation panel showing gamma ray logs, lithological logs, total organic carbon content and depths of the samples analysed.

1016 **Figure 2:** Palynostratigraphy of the Goldwyer Formation in the Canning Basin and
1017 correlation of palynozones with Unit 1, 2, 3 and 4. Modified from Quintavalle and Playford,
1018 2006.

1019 **Figure 3:** Photomicrographs of the main microfossils and cryptospores identified in Unit 4.
1020 (a) Scolecodont (worm jaw) in Goldwyer-1, 873.9–876.6 m, (b) chitinozoan in Goldwyer-1,
1021 873.9–876.6 m, (c) graptolite in Goldwyer-1, 873.9–876.6 m, (d) spinose acritarch in Theia-
1022 1, 1217.67–1217.7 m, (e) acritarch *Pireia sp A* in Theia-1, 1217.67–1217.7 m, (f) acritarch
1023 *Veryhachium sp. cf. oklahomense* in Theia-1, 1217.67–1217.7 m, (g) *Gloeocapsomorpha*
1024 *prisca* colony in Santalum-1A, 449.7–449.8 m, (h) cryptospore with what appears to be a
1025 trilete mark in Theia-1, 1217.67–1217.7 m, and (i) enclosed tetrad in Theia-1, 1217.67–
1026 1217.7 m.

1027 **Figure 4:** Photomicrographs taken under white light and, where specified, UV light using oil
1028 immersion. (a) Telalginite derived from *G. prisca* in Santalum-1A, 449.7–449.8 m, under
1029 white and fluorescent light, (b) Telalginite derived from *G. prisca*, lamalginite and
1030 liptodetrinite in Solanum-1, 296.4–296.6 m, under fluorescent light, (c) Telalginite derived
1031 from *G. prisca* in Solanum-1, 302.8–303.0 m, and (d) periderm layering in a graptolite in
1032 Goldwyer-1, 972.7–975.7 m.

1033 **Figure 5:** Chromatograms (m/z 57) showing the n -alkane distributions in the lower (Units
1034 1+2) and upper (Unit 4) Goldwyer Formation. (a) Solanum-1, 315.58–315.59 m, (b)
1035 Santalum-1A, 478.2–478.4 m, (c) Goldwyer-1, 873.9–876.6 m, (d) Goldwyer-1, 980.0–
1036 983.6 m, (e) Theia-1, 1271.48–1271.52 m, and (f) Theia-1, 1552.70–1552.75 m.

1037 **Figure 6:** MRM transitions showing C_{30} steranes and C_{30} methylsteranes identified in
1038 selected samples. Identification based on an oil standard and Grosjean et al., (2009).

1039 **Figure 7:** Biomarker differences between the lower (Units 1+2) and upper (Unit 4) Goldwyer
1040 Formation as shown by (a) Pr/Ph versus gammacerane index, (b) Pr/Ph versus DBT/P, and (c)
1041 H/St versus 2MeH/3MeH.

1042 **Figure 8:** Depth profiles in Solanum-1 of TOC content and selected molecular parameters
1043 indicative of microbial communities through the upper (Unit 4) Goldwyer Formation.

1044 **Figure 9:** Graphical representation of the microbial community during deposition of unit 4.

1045 **Figure 10:** Relative abundances of *n*-alkanes and $\delta^{13}\text{C}$ of selected samples from Solanum-1
1046 showing relatively depleted *n*-alkane $\delta^{13}\text{C}$ when the *G. prisca*-derived C_{15} – C_{19} OEP becomes
1047 predominant. $\delta^{13}\text{C}$ values provided in Table 4.

1048 **Figure 11:** $\delta^{13}\text{C}$ values of *n*-alkanes from Solanum-1 that exhibit the C_{15} – C_{19} OEP signature
1049 against the range observed for *G. prisca* –rich bitumens from North America.

1050 **Figure 12:** Relative abundances of *n*-alkanes and $\delta^{13}\text{C}$ of selected samples from Solanum-1
1051 and Santalum-1A showing a shift towards depleted stable carbon isotopic signatures when the
1052 mid-chain *n*-alkanes are abundant. $\delta^{13}\text{C}$ values provided in Table 4.

1053 **Figure 13:** Palaeogeographic reconstruction of the mid-Ordovician (452 Ma) centered around
1054 Australia after Wright et al. (2013). Stars represent localities of Early–Middle Ordovician
1055 cryptospores.

1056

1057 **Figure S1:** MRM mass fragmentograms showing hopane distributions in representative
1058 samples of units 1+2 and unit 4.

1059 **Figure S2:** MRM transitions showing C_{26} – C_{30} sterane distributions in representative samples
1060 of units 1+2 and unit 4. Identification is based on Abogbila et al., 2011; Grosjean et al., 2009;
1061 Holba et al., 1998; Tulipani et al., 2015.

1062 **Figure S3:** MRM transition m/z 426 \rightarrow 205 highlighting the variable 2 α -methylhopane and
1063 3 β -methylhopane abundances in samples from unit 4.

1064 **Figure S4:** MRM chromatograms showing methylhopanes in a sample from Solanum-1
1065 (311.0–311.1m). MeH = methylhopane.

1066 **Figure S5:** $\delta^{13}\text{C}$ values of mid-chain *n*-alkanes and short-chain *n*-alkanes in Santalum-1A,
1067 and Solanum-1.

1068 **Figure S6:** Organic-rich shales in the upper (Unit 4) Goldwyer Formation in Solanum-1
1069 imaged by the Hylogger™, core tray 52, 315.6–321.8 m.
1070

Table 1

		UNIT 4				UNITS 1+2		
		Goldwyer-1 873.86-876.61m	Theia-1 1217.67-1217.7m	Santalum-1A 449.7-489.6m*	Solanum-1 302.84-319m*	Goldwyer-1 972.65-975.66m	Theia-1 1498.8-1498.85m	Theia-1 1552.7-1552.75m
ACRITARCHA (spinose acritarchs)	<i>Rhopaliophora</i> spp.	X	X					
	<i>Michrystidium</i> sp.	X	X					
	<i>Multiplicisphaeridium</i> sp?		X					
	<i>Veryhachium</i> sp. cf. <i>oklahomense</i>		X					
	<i>Dasydorus cirritus</i>		X					
	<i>Pirea</i> sp A		X					
	<i>Ammonnidium aduncum</i>		X					
PRASINOPHYCEAE green algae	<i>Leiosphaeridia</i> sp.				X	X		
?CYANOPHYCEAE cyanobacteria	<i>G. prisca</i>		X	X**	X ₍₁₎			
OTHER ORGANIC-WALLED MICROFOSSILS (animal)								
	chitinozoans	X	X	X	X	X	X	X
	scolecodonts	X	X					
	graptolite fragments	X					X	X
CRYPTOSPORES Plant	enclosed dyads		X					
	enclosed tetrads		X					
	naked ?trilete		X					

*Santalum-1A samples: 449.7–449.8 m, 459.3–459.4 m, 489.5–489.6 m, Solanum-1 samples: 302.84–303 m, 313.4–313.5 m, 311–311.12 m, 318.9–319 m

**X: dominant >95% of assemblage, X₍₁₎: dominant in sample from 318.9–319 m

Table 2

Well	Upper Depth (m)	Lower Depth (m)	Unit	Lithology	TOC (wt. %)	HI (mg HC/g TOC)	OI (mg CO ₂ /g TOC)	Tmax (°C)	C ₃₁ H (S/S+R)	C ₂₉ $\alpha\alpha\alpha$ St S/(S+R)	dia St/(dia+reg St)	MPI	Mean Faunal Reflectance (%)	Mean Bitumen Reflectance (%)
Solanum-1	280.0	280.2	4	Carbonate	0.30	16	241	421	0.60	0.42	0.42	n.d.	n.d.	0.41
Solanum-1	284.5	284.6	4	Carbonate	0.27	93	142	440	0.59	0.45	0.44	0.39	n.d.	n.d.
Solanum-1	291.6	291.8	4	Carbonate	0.26	62	146	435	0.59	0.48	0.39	0.39	n.d.	n.d.
Solanum-1	296.4	296.6	4	Carbonate	0.37	110	98	435	0.59	0.50	0.39	0.42	0.71	n.d.
Solanum-1	302.8	303.0	4	Carbonate	0.34	89	136	434	0.58	0.49	0.41	0.39	0.68	0.40
Solanum-1	304.7	304.8	4	Carbonate	0.18	158	120	436	0.63	0.54	0.50	n.d.	n.d.	n.d.
Solanum-1	308.8	308.9	4	Carbonate	0.37	435	55	439	0.59	0.54	0.46	n.d.	n.d.	n.d.
Solanum-1	310.3	310.4	4	Carbonate	0.1	129	230	432	0.61	0.56	0.45	n.d.	n.d.	n.d.
Solanum-1	311.0	311.1	4	Carb/Mudst	0.96	480	36	441	0.59	0.48	0.46	0.24	n.d.	n.d.
Solanum-1	313.4	313.5	4	Carbonate	0.21	74	133	432	0.58	0.49	0.35	0.34	n.d.	n.d.
Solanum-1	315.6	315.6	4	Mudstone	3.58	763	9	438	0.59	0.53	0.58	0.21	n.d.	n.d.
Solanum-1	316.2	316.3	4	Carb/Mudst	0.58	244	99	437	0.60	0.51	0.46	n.d.	n.d.	n.d.
Solanum-1	318.9	319.0	4	Carb/Mudst	1.32	377	22	437	0.58	0.43	0.47	0.28	0.53	n.d.
Santalum-1A	449.7	449.8	4	Carbonate	0.39	131	144	431	n.d.	n.d.	n.d.	n.d.	n.d.	n.d.
Santalum-1A	459.3	459.4	4	Carbonate	0.42	8	89	420	n.d.	n.d.	n.d.	n.d.	n.d.	n.d.
Santalum-1A	466.6	466.7	4	Carbonate	0.26	38	183	425	0.55	0.28	0.35	0.53	0.60	n.d.
Santalum-1A	470.8	470.9	4	Carbonate	0.16	20	275	421	0.53	0.45	0.41	n.d.	n.d.	n.d.
Santalum-1A	474.6	474.7	4	Carbonate	0.11	148	198	429	0.53	0.42	0.44	n.d.	n.d.	n.d.
Santalum-1A	478.2	478.4	4	Carbonate	0.46	147	98	434	0.58	0.26	0.42	0.45	n.d.	n.d.
Santalum-1A	485.3	485.4	4	Carbonate	0.24	28	197	423	0.50	0.28	0.38	n.d.	n.d.	n.d.
Santalum-1A	489.5	489.6	4	Carbonate	0.33	267	117	434	0.56	0.41	0.45	n.d.	0.55	n.d.
Goldwyer-1	873.9	876.6	4	Mudstone	0.34	59	121	432	0.58	0.50	0.31	0.41	0.79	0.46
Goldwyer-1	972.7	975.7	1+2	Mudstone	1.35	214	37	434	0.54	0.51	0.59	0.40	1.05	0.79
Goldwyer-1	975.7	980.0	1+2	Mudstone	0.35	114	131	435	0.59	0.44	0.60	n.d.	n.d.	n.d.

Goldwyer-1	980.0	983.6	1+2	Mudstone	1.37	232	29	439	0.57	0.52	0.60	0.42	1.05	0.80
Theia-1	1217.7	1217.7	4	Silty Mudst.	n.d.	n.d.	n.d.	n.d.	n.d.	n.d.	n.d.	n.d.	n.d.	n.d.
Theia-1	1271.5	1271.5	4	Silty Mudst.	0.06	n.d.	n.d.	n.d.	n.d.	n.d.	n.d.	n.d.	n.d.	n.d.
Theia-1**	1276.1	1276.2	4	Silty Mudst.	n.d.	n.d.	n.d.	n.d.	n.d.	n.d.	n.d.	n.d.	n.d.	n.d.
Theia-1**	1518.3	1518.3	1+2	Silty Mudst.	n.d.	n.d.	n.d.	n.d.	n.d.	n.d.	n.d.	0.48	n.d.	n.d.
Theia-1**	1523.6	1523.6	1+2	Silty Mudst.	1.92	153	30	438	n.d.	n.d.	n.d.	0.49	n.d.	1.05
Theia-1**	1538.3	1538.3	1+2	Silty Mudst.	2.18	149	24	436	n.d.	n.d.	n.d.	0.52	1.29	1.13
Theia-1**	1547.1	1547.1	1+2	Silty Mudst.	3.08	154	18	435	n.d.	n.d.	n.d.	0.53	1.30	1.05
Theia-1	1552.7	1552.8	1+2	Silty Mudst.	3.15	214	11	441	n.d.	n.d.	n.d.	0.52	n.d.	n.d.
Theia-1**	1553.6	1553.6	1+2	Silty Mudst.	3.67	166	11	433	n.d.	n.d.	n.d.	0.56	1.28	1.17

*analyses performed on cuttings

**data courtesy of FINDER Exploration Pty Ltd

n.d. = not determined, Mudst = mudstone

$C_{31}H\ S/(S+R) = C_{31}\ \text{homohopane}\ 22S/(22S+22R)$

$C_{29}\ \alpha\alpha\alpha\ S/(S+R) = C_{29}\ 5\alpha,14\alpha,17\alpha\ \text{sterane}\ 20S/(20S+20R)$

$\text{Dia St}/(\text{dia}+\text{reg St}) = \Sigma C_{27}-C_{29}\ \text{diasteranes} / \Sigma C_{27}-C_{29}\ \text{diasteranes} + \Sigma C_{27}-C_{29}\ \text{regular steranes}$

$\text{MPI (methylphenanthrene index)} = (3\text{-MP}+2\text{-MP})/(3\text{-MP}+2\text{-MP}+9\text{-MP}+1\text{-MP})$

Mean faunal reflectance = average of chitinozoan and graptolite maceral reflectance

Mean bitumen reflectance = average of bitumen maceral reflectance

Table 3

Molecular signature	Identified in	Biological & environmental interpretation	Further info & references
OEP <i>n</i> -C ₁₅ to <i>n</i> -C ₁₉	Solanum-1 (311m, 316-319m), Theia-1 (1271.5m)	<i>Gloeocapsomorpha prisca</i> , marine organism of uncertain affinity	Hoffman et al. (1987), Blokker et al. (2001)
Mid to long chain (C ₂₃ –C ₃₂) <i>n</i> -alkanes	Santalum-1A	plant inputs (bryophytes or aquatic macrophytes)	Ficken et al. (2000)
C ₃₀ -hopanes, homohopanes	all samples, at varying abundances	diagnostic for Bacteria	Brocks and Summons (2014)
2 α -methylhopanes	all samples, at varying abundances	generally diagnostic for cyanobacteria in Phanerozoic marine deposits	Summons et al. (1999) Ricci et al. (2014, 2015)
3 β -methylhopanes	all samples, at varying abundances	diagnostic for certain methylotrophs, methanotrophs and acetic acid bacteria	Summons and Jahnke (1990) Welander and Summons (2012)
Gammacerane	all samples, higher abundance in Goldwyer-1 (973-984m)	water column stratification	Sinninghe Damsté et al. (1995)
C ₂₇ –C ₂₉ steranes	all samples, at varying abundances	primarily diagnostic for eukaryotes in marine deposits	Brocks and Summons, 2014
24- <i>n</i> -propylcholestane	Solanum-1, Goldwyer-1 (874-876m)	Pelagophyte algae, a biomarker for marine conditions	Moldowan et al. (1990)
OEP long-chain alkyl-naphthalenes (C ₂₁ , C ₂₃)	Solanum-1 (280-319m), Santalum-1A (449.7m)	<i>Gloeocapsomorpha prisca</i> , marine organism of uncertain affinity	Fowler et al. (2004)
Benzonaphthofurans	Theia-1 (1217.6m)	? Plant derived	Li and Ellis (2015)
Isorenieratane, Palaerenieratane	Solanum-1 (316.2-316.3m), Theia-1 (1552.7-1552.75m)	Green sulphur bacteria, photic zone euxinia	Brocks and Summons (2014)
Isotopic signature			
¹³ C depleted <i>n</i> -C ₁₇ and <i>n</i> -C ₁₉ (-31.4‰) compared to <i>n</i> -C ₁₆ and <i>n</i> -C ₁₈ (-30.0‰)	Solanum-1 (311m, 316-319m)	<i>G. prisca</i> utilised a ¹³ C depleted carbon source (possibly from methanotrophs)	
¹³ C depleted <i>n</i> -C ₂₃₋₃₂ relative to <i>n</i> -C ₁₆₋₁₉	Santalum-1A	isotopic discrepancy greater than in other samples, attributed to a (land) plant input	

Table 4

Well	Upper Depth (m)	Unit	Pr/Ph	OEP (C ₁₃ - C ₃₀)	hopanes (C ₂₇ -C ₃₅)/steranes (C ₂₇ -C ₂₉)	Gamma cerane index (Ga/C ₃₁ H22R)	2MHI (%)	3MHI (%)	2MeH/3MeH (C ₃₁ -C ₃₅)	C ₃₅ homohopane index	DNH/30H	TNH/ (Ts+ Tm)	DBT/ P	C27 St	C28 St	C29 St
Solanum-1	280.04	4	0.6	0.8	12.5	0.01	7.8	7.7	1.13	0.02	0.06	0.01	n.d.	0.43	0.19	0.39
Solanum-1	284.50	4	0.8	1.1	12.3	0.01	7.4	12.2	0.67	0.03	0.06	0.01	n.d.	0.39	0.19	0.41
Solanum-1	291.60	4	0.5	1.0	3.5	0.07	10.3	7.0	1.73	0.05	0.13	0.03	0.13	0.40	0.23	0.37
Solanum-1	296.40	4	0.6	1.0	2.6	0.09	11.7	7.2	1.98	0.07	0.15	0.04	0.11	0.38	0.25	0.37
Solanum-1	302.84	4	0.3	1.0	3.1	0.06	8.8	9.6	1.01	0.05	0.14	0.03	0.07	0.43	0.23	0.34
Solanum-1	304.73	4	0.7	1.0	4.9	0.08	6.5	5.2	1.27	n.d.	0.10	n.d.	n.d.	0.40	0.27	0.34
Solanum-1	308.79	4	0.5	1.2	5.6	0.03	5.9	9.5	0.60	0.02	0.08	0.01	0.06	0.49	0.17	0.34
Solanum-1	310.30	4	0.6	1.0	6.6	0.04	7.5	5.8	1.32	0.02	0.08	n.d.	n.d.	0.49	0.17	0.34
Solanum-1	311.00	4	0.9	1.4	8.5	0.01	7.2	14.9	0.52	0.04	0.05	0.00	0.01	0.39	0.18	0.43
Solanum-1	313.40	4	0.4	1.0	3.0	0.08	11.5	6.6	2.04	0.08	0.13	0.04	0.08	0.36	0.25	0.39
Solanum-1	315.58	4	1.2	1.8	10.9	0.02	3.5	12.7	0.25	0.02	0.01	0.00	0.03	0.49	0.14	0.36
Solanum-1	316.20	4	1.0	1.3	6.1	0.04	3.4	9.1	0.35	0.03	0.06	0.02	0.06	0.49	0.18	0.32
Solanum-1	318.90	4	1.1	1.3	6.7	0.07	5.5	10.6	0.46	0.04	0.06	0.01	0.01	0.41	0.21	0.38
Santalum-1A	449.73	4	1.8	1.1	n.d.	n.d.	n.d.	n.d.	n.d.	n.d.	n.d.	n.d.	0.02	n.d	n.d	n.d
Santalum-1A	459.30	4	0.8	1.1	6.6	n.d.	n.d.	n.d.	n.d.	n.d.	n.d.	n.d.	n.d.	n.d	n.d	n.d
Santalum-1A	466.59	4	1.4	1.0	6.7	0.03	7.8	14.0	0.58	0.03	0.12	n.d.	n.d.	0.33	0.21	0.46
Santalum-1A	470.82	4	1.4	1.0	6.0	0.03	5.9	5.6	1.32	0.02	0.06	0.01	0.22	0.44	0.18	0.38
Santalum-1A	474.60	4	1.6	1.0	5.7	0.03	4.8	9.2	0.66	0.03	0.06	0.01	0.07	0.47	0.21	0.31
Santalum-1A	478.19	4	1.7	1.1	8.4	0.02	5.5	16.5	0.37	0.02	0.08	0.00	n.d.	0.38	0.19	0.44
Santalum-1A	485.30	4	1.0	1.0	9.2	0.02	8.1	15.7	0.54	0.03	0.10	n.d.	n.d.	0.30	0.18	0.52
Santalum-1A	489.50	4	1.7	1.0	5.2	0.05	6.7	8.9	0.76	n.d.	0.05	0.01	0.06	0.48	0.20	0.32
Goldwyer-1	873.86	4	1.8	1.0	1.8	0.09	5.1	2.5	1.95	0.03	0.18	0.03	0.03	0.50	0.27	0.22
Goldwyer-1	972.65	1+2	0.6	1.1	2.0	0.33	7.0	2.7	8.04	0.07	0.07	0	0.03	0.35	0.18	0.47

Goldwyer-1	975.66	1+2	0.9	1.1	1.5	0.36	4.5	2.2	3.86	0.03	0.04	0	n.d.	0.31	0.14	0.54
Goldwyer-1	979.97	1+2	1.0	1.1	1.5	0.73	6.7	4.6	7.08	0.07	0.13	0	0.03	0.36	0.18	0.46
Theia-1	1217.7	4	1.6	1.0	n.d.	n.d.	n.d.	n.d.	n.d.	n.d.	n.d.	n.d.	0.10	n.d.	n.d.	n.d.
Theia-1	1271.48	4	1.1	1.4	1.6	n.d.	n.d.	n.d.	n.d.	n.d.	n.d.	n.d.	0.14	n.d.	n.d.	n.d.
Theia-1**	1276.1	4	1.5	1.1	3.0	n.d.	n.d.	n.d.	n.d.	n.d.	n.d.	n.d.	0.14	n.d.	n.d.	n.d.
Theia-1**	1518.26	1+2	1.5	1.2	n.d.	n.d.	n.d.	n.d.	n.d.	n.d.	n.d.	n.d.	0.08	n.d.	n.d.	n.d.
Theia-1**	1523.56	1+2	1.1	1.1	n.d.	n.d.	n.d.	n.d.	n.d.	n.d.	n.d.	n.d.	0.06	n.d.	n.d.	n.d.
Theia-1**	1538.28	1+2	1.4	1.2	n.d.	n.d.	n.d.	n.d.	n.d.	n.d.	n.d.	n.d.	0.04	n.d.	n.d.	n.d.
Theia-1**	1547.07	1+2	1.4	1.0	n.d.	n.d.	n.d.	n.d.	n.d.	n.d.	n.d.	n.d.	0.04	n.d.	n.d.	n.d.
Theia-1	1552.70	1+2	1.4	1.2	n.d.	n.d.	n.d.	n.d.	n.d.	n.d.	n.d.	n.d.	0.06	n.d.	n.d.	n.d.
Theia-1**	1553.59	1+2	1.6	1.2	n.d.	n.d.	n.d.	n.d.	n.d.	n.d.	n.d.	n.d.	0.04	n.d.	n.d.	n.d.

**data courtesy of Finder Exploration Pty Ltd

n.d. = not determined

Gammacerane index = Gammacerane/C₃₁H₂₂R

2MH/3MH = 2 α -methylhopanes/3 β -methylhopanes (C₃₁ - C₃₅)

C₃₅ homohopane index = C₃₅ homohopanes/ Σ (C₃₁-C₃₅ homohopanes)

DNH/30H = 28,30-*dinor*hopane/C₃₀ 17 α ,21 β ($\alpha\beta$) hopane

TNH/(Ts+Tm) = 25,28,30-*trisnor*hopane/(18 α 22,29,30-*trisnor*hopane+17 α 22,29,30-*trisnor*hopane)

24/(24+27) *norcholestanes* = Σ 24-*norcholestanes*/ Σ (24- + 27- *norcholestanes*)

Table 5

Well	Upper Depth (m)	Short-chain <i>n</i> -alkanes								Long-chain <i>n</i> -alkanes									
		C ₁₄	C ₁₅	C ₁₆	C ₁₈	C ₁₉	C ₂₀	C ₂₁	C ₂₂	C ₂₃	C ₂₄	C ₂₅	C ₂₆	C ₂₇	C ₂₈	C ₂₉	C ₃₀	C ₃₁	C ₃₂
Santalum-1A	459.3				-27.1	-27.8	-27.7	-27.4	-28.2	-29.3		-31.1							
Santalum-1A	466.6		-28.8	-27.7	-28.3	-27.9	-27.6	-28.1	-28.4	-28.4	-29.4	-30.1	-29.9	-30.3	-30.5	-31.1		-32.1	-32.3
Santalum-1A	470.8			-27.8		-27.7	-27.7	-28.1	-28.6	-29.2	-30.0	-30.7			-30.7	-31.0			
Santalum-1A	474.6	-29.2		-27.2		-27.8	-27.3			-30.5	-31.0	-31.8	-31.8	-31.5	-31.7		-31.6	-32.1	-32.5
Santalum-1A	478.2	-28.2	-27.7	-27.1	-27.9	-29.4		-29.5	-30.7	-31.9	-31.5	-32.0	-31.2	-31.5		-32.0	-32.0	-31.7	
Santalum-1A	485.3		-28.8	-27.8	-27.4	-28.1	-28.4		-29.7		-30.9	-30.5		-30.6		-30.9		-31.4	
Solanum-1	280.0				-27.8	-28.5	-29.1		-29.0	-29.5									
Solanum-1	291.6					-28.3	-27.9		-28.1										
Solanum-1	296.4			-28.6	-27.8	-28.4	-28.4	-27.6		-27.6			-27.6	-28.6					
Solanum-1	302.8				-28.5			-28.8	-28.7	-28.2	-29.7	-29.7							
Solanum-1*	311.0	-31.6	-31.6	-30.0	-31.3	-30.1	-31.5	-30.5											
Solanum-1	313.4				-27.9		-28.5					-28.9			-28.3				
Solanum-1*	315.6	-31.9	-31.6	-30.3		-31.4													
Solanum-1	316.2		-30.4	-30.3		-30.2	-29.7												
Solanum-1*	318.9	-31.3	-31.4	-31.0	-30.2	-31.3	-30.0	-30.4											
Goldwyer-1	873.9		-29.1	-28.5	-28.4	-29.0	-29.2			-30.0									
Goldwyer-1	972.7	-31.9	-32.2	-31.7	-31.7	-32.1	-33.0	-33.5	-32.7	-33.8		-32.6							
Goldwyer-1	980.0	-32.2	-32.3	-31.4			-32.4	-32.6		-32.2	-32.4	-32.7	-32.3		-32.4				
Theia 1	1557.2	-32.0		-32.5		-31.1	-31.9	-31.9		-33.0	-33.7	-33.4							

* $\delta^{13}\text{C}$ could be measured due to extremely low abundance of pristane, data is shown in figure 12. In all other samples *n*-C₁₇ co-eluted with pristane

Table 6

Well	Upper Depth (m)	Unit	$\delta^{13}\text{C}$ (<i>n</i> - C ₁₆₋₁₉)	$\delta^{13}\text{C}$ (<i>n</i> - C ₂₃₋₃₂)	Δ
Santalum-1A	459.3	4	-27.5	-30.2	2.8
Santalum-1A	466.6	4	-27.9	-30.2	2.3
Santalum-1A	470.8	4	-27.7	-30.3	2.6
Santalum-1A	474.6	4	-27.5	-31.5	4.0
Santalum-1A	478.2	4	-28.2	-31.7	3.6
Santalum-1A	485.3	4	-27.8	-30.9	3.1
Solanum-1	280.0	4	-28.2	-29.5	1.3
Solanum-1	291.6	4	-28.3		
Solanum-1	296.4	4	-28.3	-27.9	-0.3
Solanum-1	302.8	4	-28.5	-29.2	0.7
Solanum-1	313.4	4	-27.9	-28.6	0.7
Solanum-1	311.0	4	-30.5		NA*
Solanum-1	315.6	4	-30.8		NA*
Solanum-1	316.2	4	-30.2		NA*
Solanum-1	318.9	4	-30.8		NA*
Goldwyer-1	873.9	4	-28.6	-30.0	1.3
Goldwyer-1	972.7	1+2	-31.8	-33.2	1.4
Goldwyer-1	980.0	1+2	-31.4	-32.4	0.9
Theia-1	1557.2	1+2	-31.8	-33.3	1.5

NA = not applicable, these samples display a strong *G. prisca* *n*-alkane signature (Fig. 4a)

Figures

Figure 1

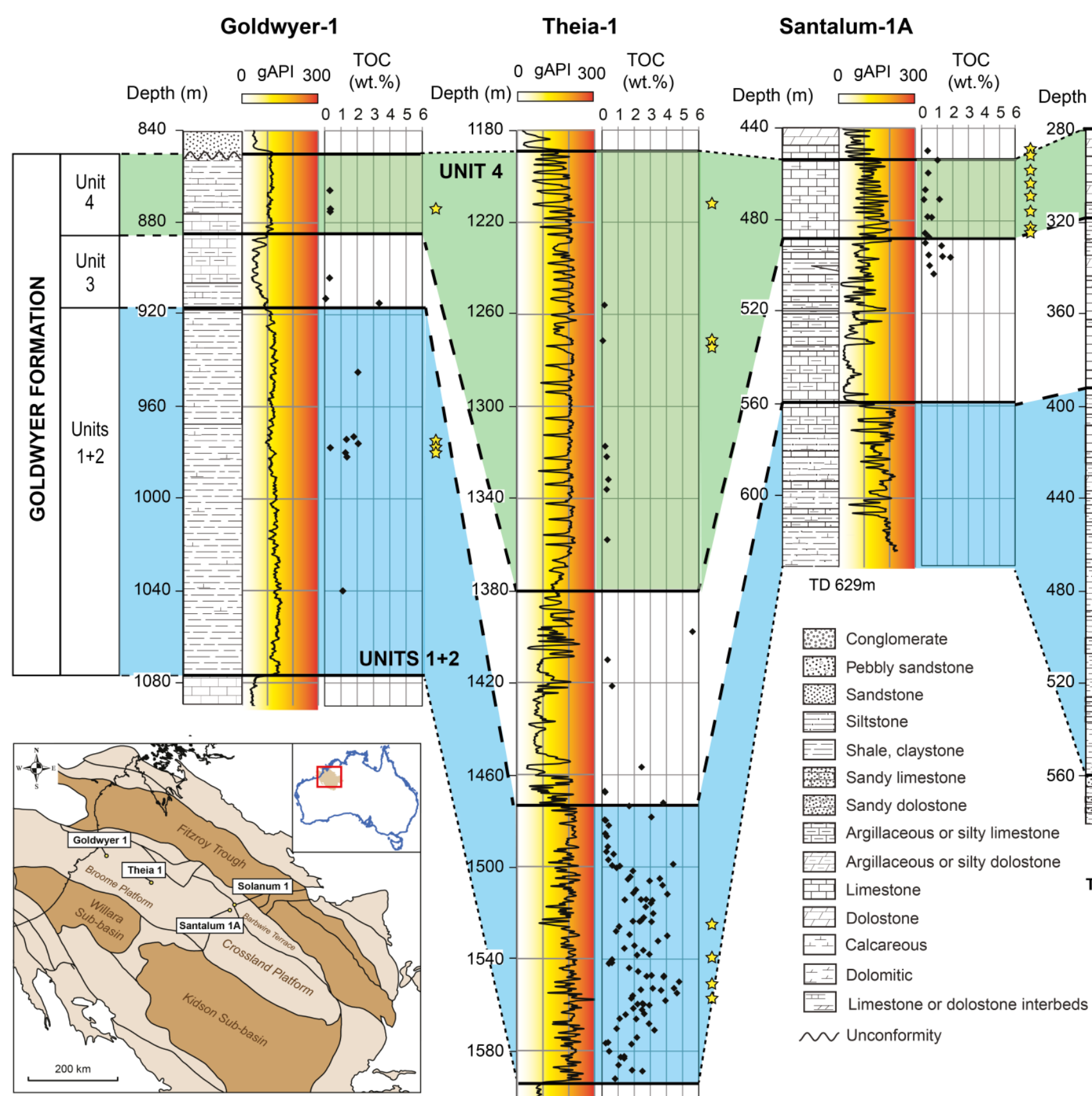


Figure 2

	Conodont zonation W. Australia	Canning Basin Formations		PALYNOZONES		Chitinozoan zonation Laurentia
				Acritarchs	Chitinozoans	
DARRIWILIAN	<i>Phragmodus- Plectodina</i>	NITA				
	<i>Histiodella holodentata</i>	GOLDWYER	Unit 4	<i>Dactylofusa striatogranulata</i>	<i>Belonechitina micracantha</i>	----- <i>Cyathochitina jenkinsi</i>
			Unit 3	<i>Aremoricanium solaris</i>	<i>Conochitina subcylindrica</i>	----- <i>Rhabdochitina turgida- Conochitina subcylindrica</i>
			Unit 2			
			Unit 1	<i>Sacculidium aduncum</i>	<i>Conchitina langei</i>	----- <i>Lagenochitina pirum</i>
				<i>Comasphaeridium setaricum</i>	<i>Lagenochitina combazi</i>	-----

Figure 3

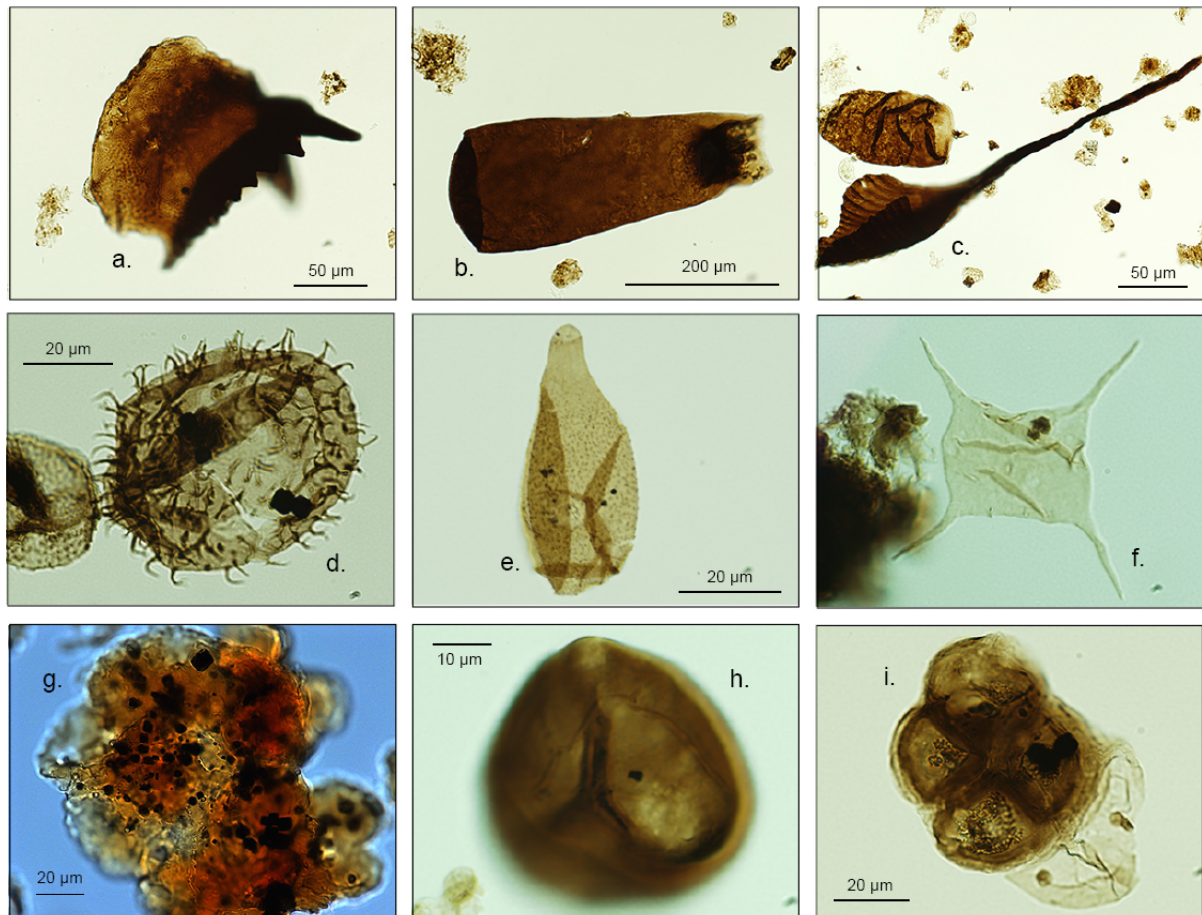


Figure 4

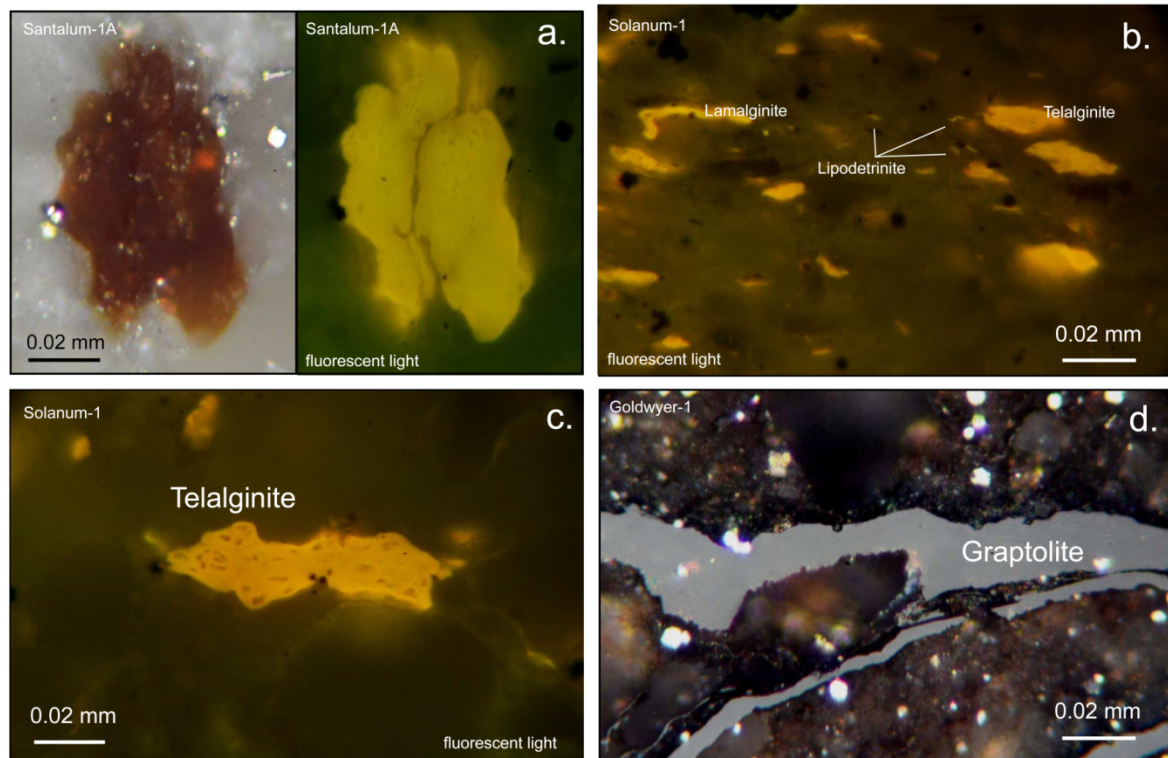


Figure 5

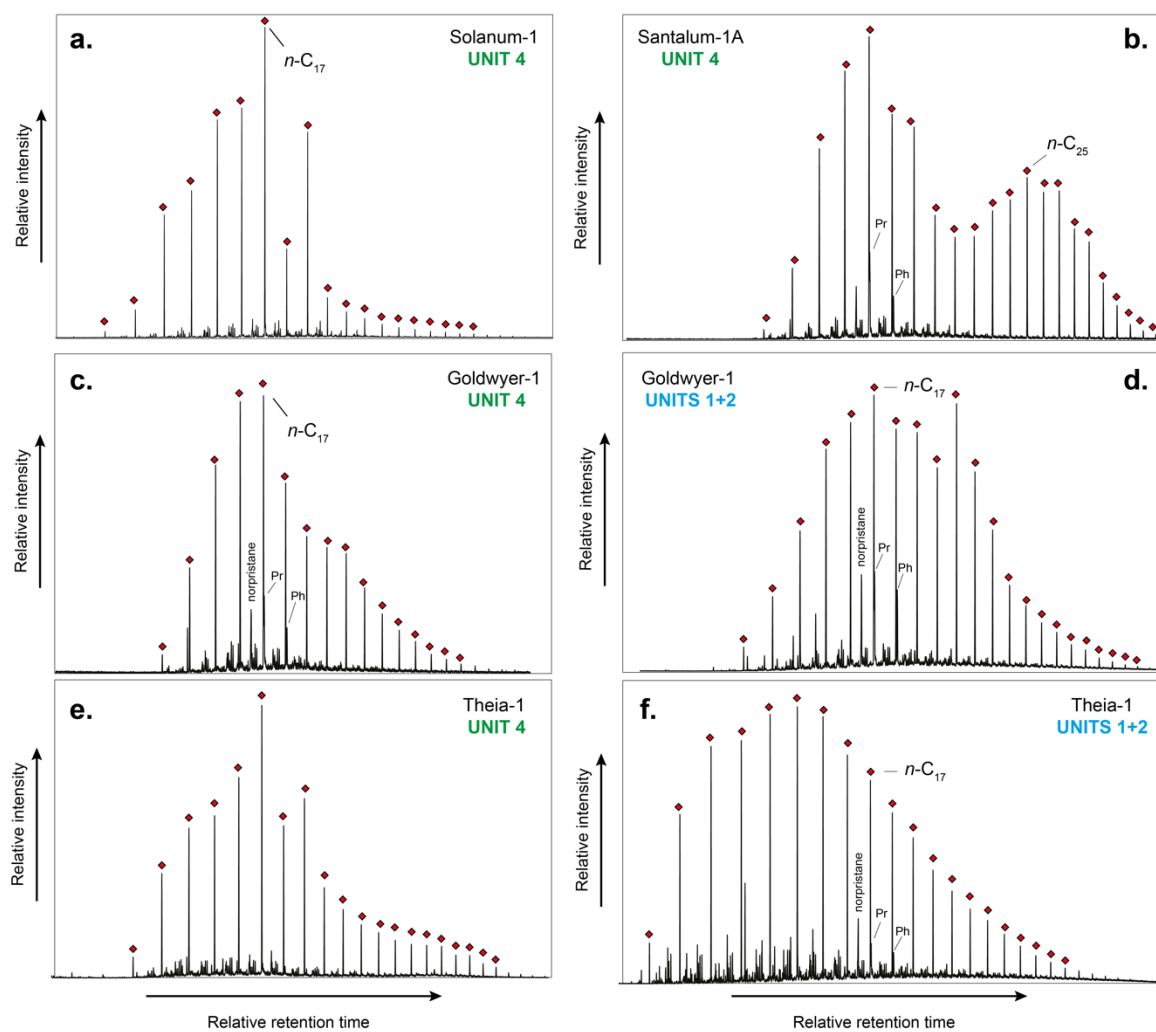


Figure 6

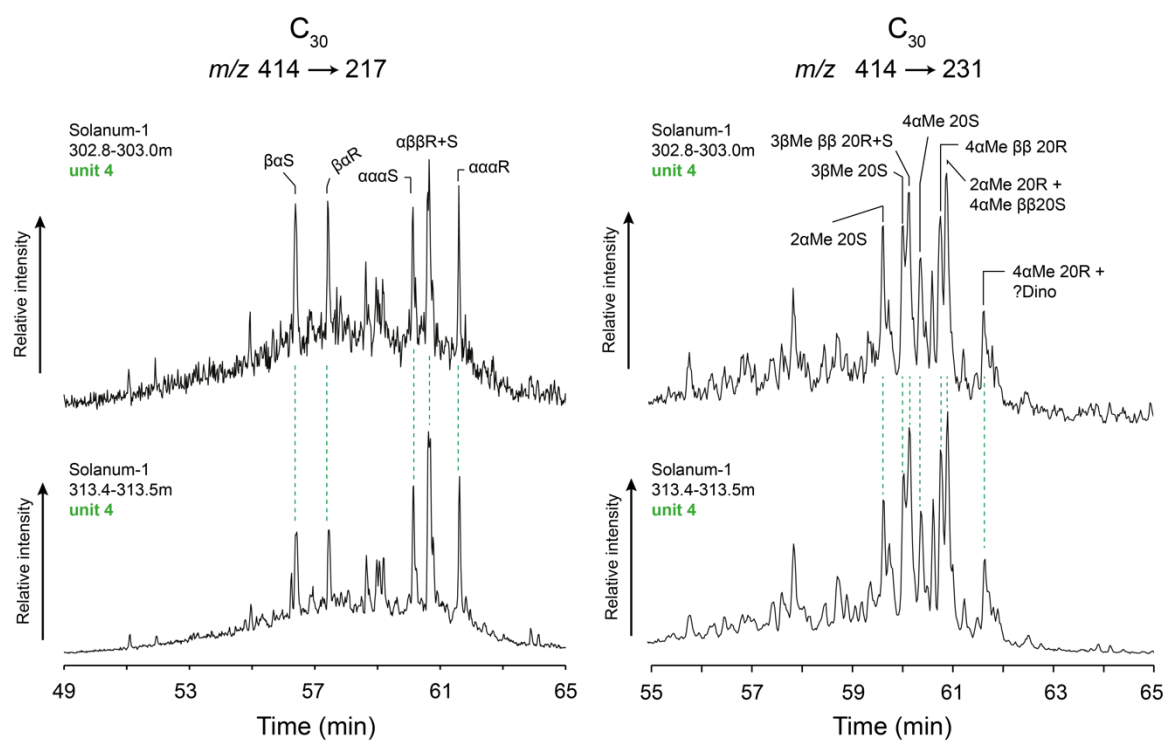


Figure 7

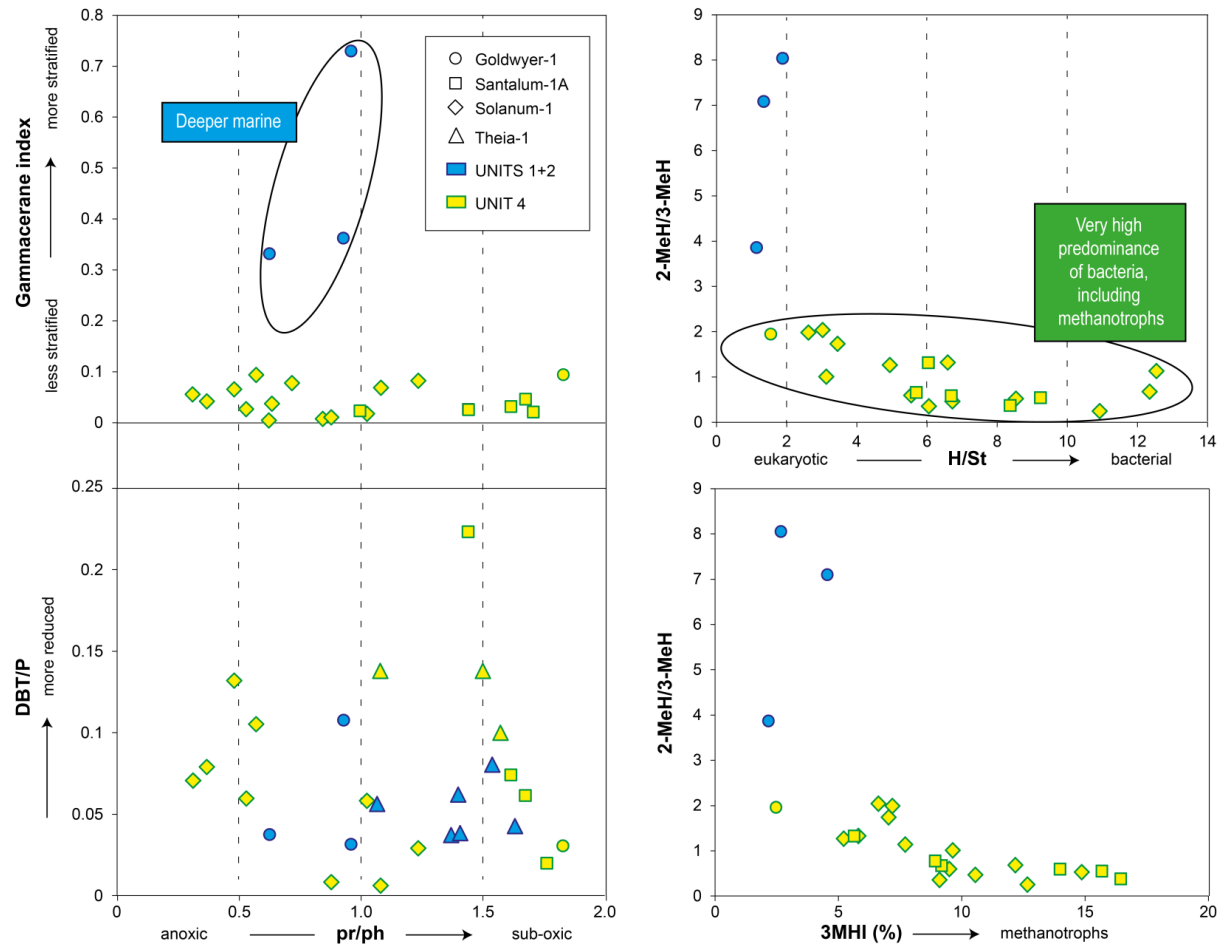


Figure 8

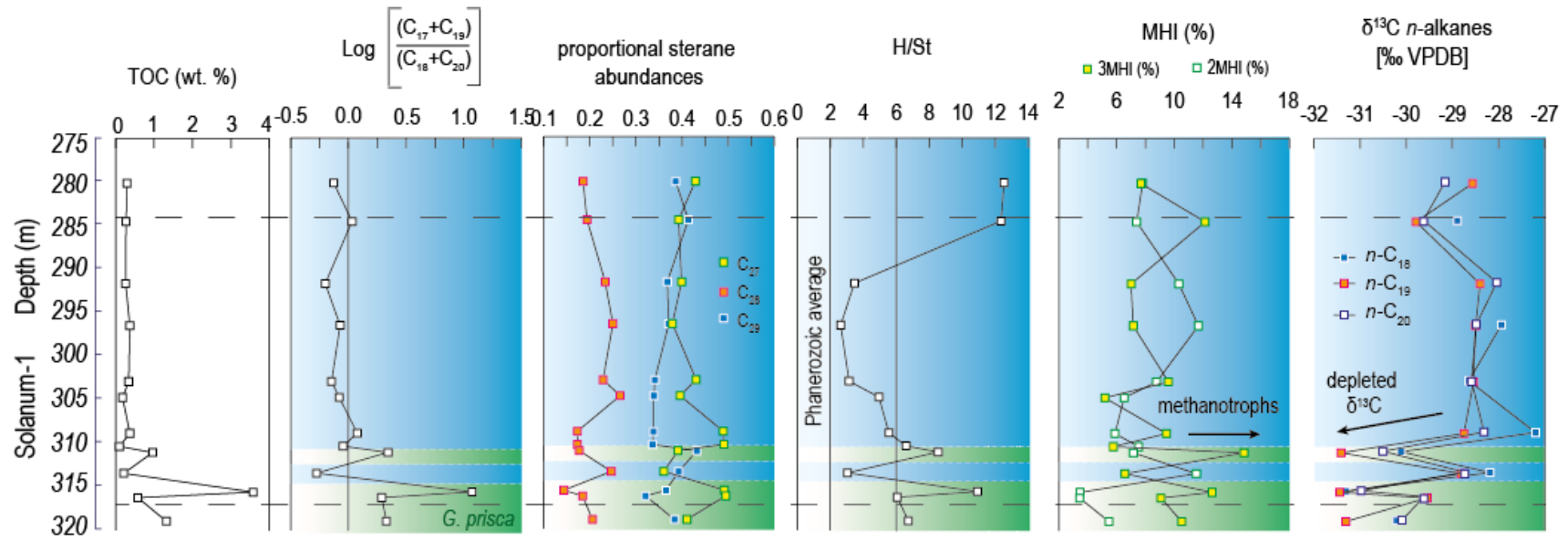


Figure 9

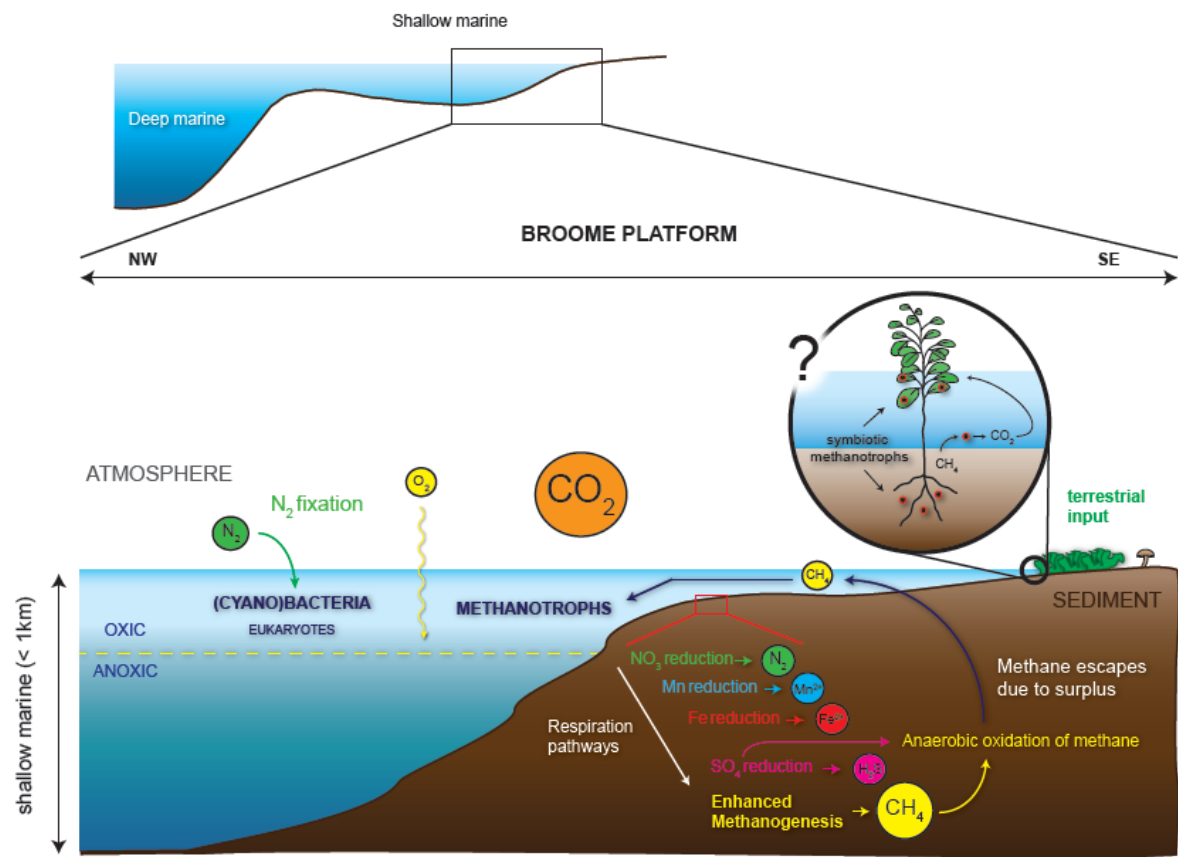


Fig 10

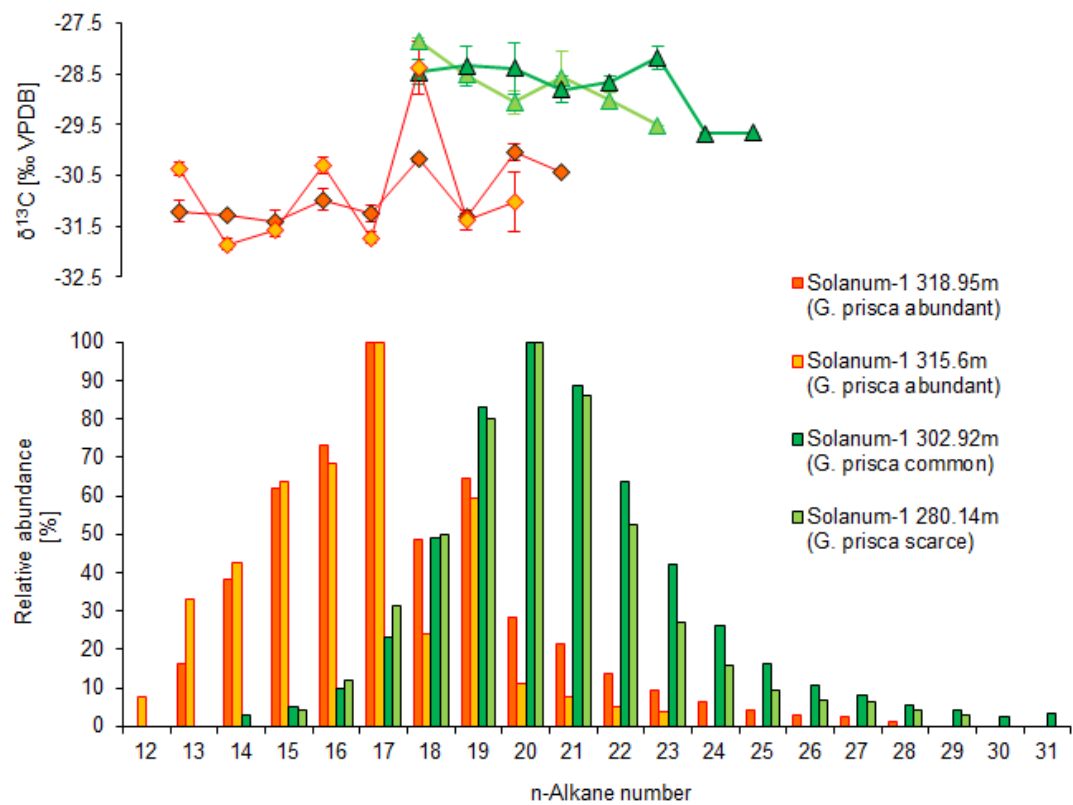


Figure 11

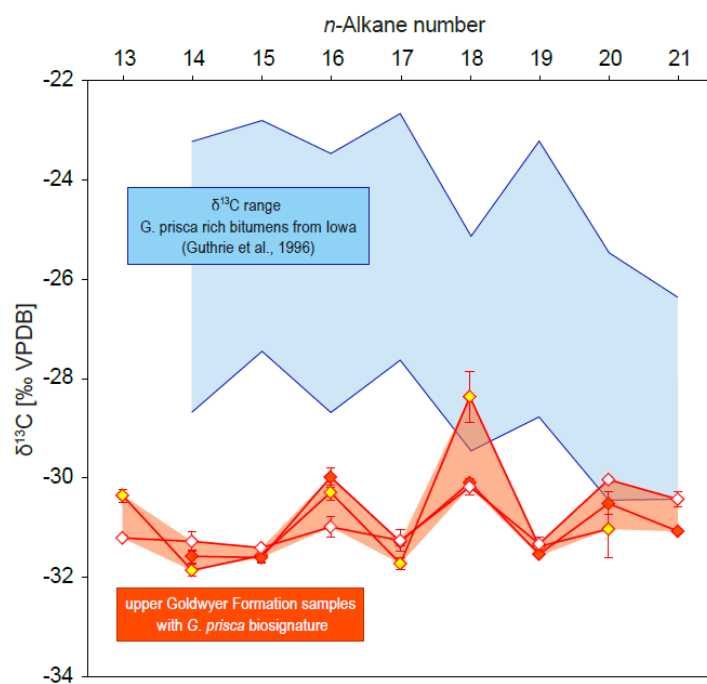


Figure 12

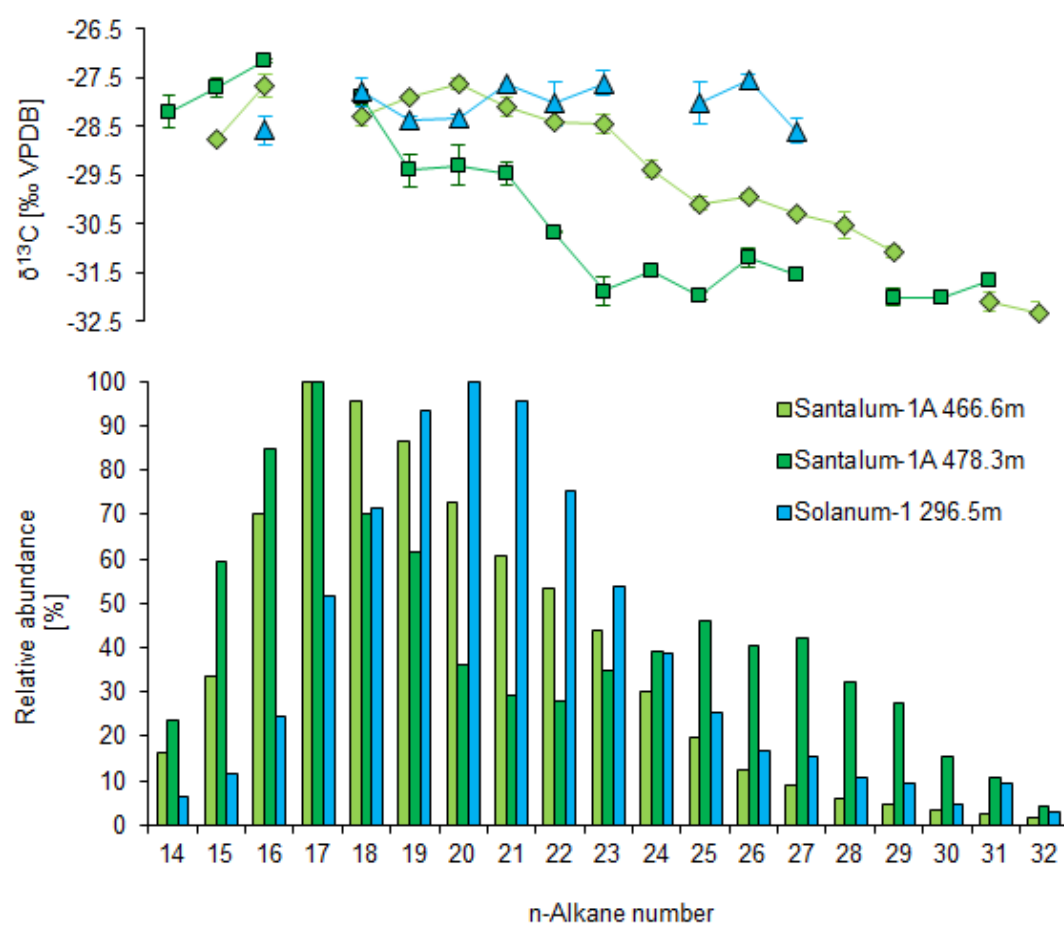


Figure 13

